Journal of Enzyme Inhibition and Medicinal Chemistry

ISSN: 1475-6366 (Print) 1475-6374 (Online) Journal homepage: http://www.tandfonline.com/loi/ienz20

The role of 5-arylalkylamino- and 5-piperazino-moieties on the 7-aminopyrazolo[4,3-d]pyrimidine core in affecting adenosine A_1 and A_{2A} receptor affinity and selectivity profiles

Lucia Squarcialupi, Marco Betti, Daniela Catarzi, Flavia Varano, Matteo Falsini, Annalisa Ravani, Silvia Pasquini, Fabrizio Vincenzi, Veronica Salmaso, Mattia Sturlese, Katia Varani, Stefano Moro & Vittoria Colotta

To cite this article: Lucia Squarcialupi, Marco Betti, Daniela Catarzi, Flavia Varano, Matteo Falsini, Annalisa Ravani, Silvia Pasquini, Fabrizio Vincenzi, Veronica Salmaso, Mattia Sturlese, Katia Varani, Stefano Moro & Vittoria Colotta (2017) The role of 5-arylalkylamino- and 5-piperazino- moieties on the 7-aminopyrazolo[4,3-d]pyrimidine core in affecting adenosine A_1 and A_{2A} receptor affinity and selectivity profiles, Journal of Enzyme Inhibition and Medicinal Chemistry, 32:1, 248-263, DOI: 10.1080/14756366.2016.1247060

To link to this article: http://dx.doi.org/10.1080/14756366.2016.1247060

JOURNAL OF ENZYME INHIBITION AND MEDICINAL CHEMISTRY, 2017
VOL. 32, NO. 1, 248–263
http://dx.doi.org/10.1080/14756366.2016.1247060

Taylor & Francis
Taylor & Francis Group

RESEARCH ARTICLE

OPEN ACCESS

The role of 5-arylalkylamino- and 5-piperazino- moieties on the 7-aminopyrazolo[4,3-*d*]pyrimidine core in affecting adenosine A_1 and A_{2A} receptor affinity and selectivity profiles

Lucia Squarcialupi[a], Marco Betti[a], Daniela Catarzi[a], Flavia Varano[a], Matteo Falsini[a], Annalisa Ravani[b], Silvia Pasquini[b], Fabrizio Vincenzi[b], Veronica Salmaso[c], Mattia Sturlese[c], Katia Varani[b], Stefano Moro[c] and Vittoria Colotta[a]

[a]Dipartimento di Neuroscienze, Psicologia, Area del Farmaco e Salute del Bambino, Sezione di Farmaceutica e Nutraceutica, Università di Firenze, Sesto Fiorentino, Italy; [b]Dipartimento di Scienze Mediche, Sezione di Farmacologia, Università di Ferrara, Ferrara, Italy; [c]Molecular Modeling Section (MMS), Dipartimento di Scienze del Farmaco, Università di Padova, Padova, Italy

ABSTRACT

New 7-amino-2-phenylpyrazolo[4,3-*d*]pyrimidine derivatives, substituted at the 5-position with aryl(alkyl)amino- and 4-substituted-piperazin-1-yl- moieties, were synthesized with the aim of targeting human (h) adenosine A_1 and/or A_{2A} receptor subtypes. On the whole, the novel derivatives **1**–**24** shared scarce or no affinities for the off-target hA_{2B} and hA_3 ARs. The 5-(4-hydroxyphenethylamino)- derivative **12** showed both good affinity ($K_i = 150$ nM) and the best selectivity for the hA_{2A} AR while the 5-benzylamino-substituted **5** displayed the best combined hA_{2A} ($K_i = 123$ nM) and A_1 AR affinity ($K_i = 25$ nM). The 5-phenethylamino moiety (compound **6**) achieved nanomolar affinity ($K_i = 11$ nM) and good selectivity for the hA_1 AR. The 5-(N^4-substituted-piperazin-1-yl) derivatives **15**–**24** bind the hA_1 AR subtype with affinities falling in the high nanomolar range. A structure-based molecular modeling study was conducted to rationalize the experimental binding data from a molecular point of view using both molecular docking studies and Interaction Energy Fingerprints (IEFs) analysis.

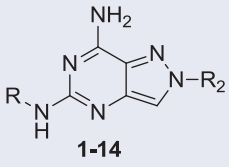

1-14

R_2= Ph, Me, CH_2Ph
R= Ph, $(CH_2)_{1\text{-}3}$-Ar

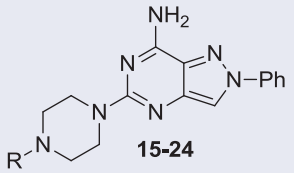

15-24

R= Ph, $(CH_2)_{1,2}$-Ar, COR_1

ARTICLE HISTORY
Received 3 August 2016
Revised 3 October 2016
Accepted 4 October 2016

KEYWORDS
Adenosine A1 and A2A receptor antagonists; G protein-coupled receptors; ligand-receptor modeling studies; pyrazolo[4,3-d]pyrimidines

Introduction

Adenosine receptors (ARs) are classified as A_1, A_{2A}, A_{2B} and A_3 subtypes[1,2] and typically inhibit (A_1 and A_3) or activate (A_{2A} and A_{2B}) adenylyl cyclase. A_1 receptor is highly expressed in brain areas, such as the hippocampus and prefrontal cortex[3,4], implicated in the control of emotions and cognition functions. Therefore, A_1 AR antagonists are investigated as therapeutic agents for mental dysfunctions, such as dementia and anxiety[3–5]. The A_{2A} AR subtype is present in the brain with the highest concentration in the striatum, nucleus accumbens, hippocampus and cortex, and its blockade has proven to be effective in neurodegenerative pathologies such as Parkinson's disease (PD)[6–8]. The A_{2A} AR antagonist istradefylline has been recently approved for marketing in Japan for the treatment of PD patients[9]. In preclinical studies, dual A_1/A_{2A} antagonists have also turned out to be useful for PD therapy because they reduce both motor (A_{2A}) and cognitive (A_1) impairment associated with this pathology[5,10–12].

Recent studies have highlighted new therapeutic applications of A_{2A} AR antagonists[12]. If topically administered, they diminish scar size and promote restoration of skin integrity[13]. A_{2A} AR antagonists have also demonstrated efficacy in enhancing immunologic response, especially by markedly improving anti-tumor immunity in mouse models, thus promoting tumor regression. A_{2A} AR antagonists have been shown to improve the effect of tumor vaccines during T-cell activation, and may work in concert with other immune checkpoint inhibitors in cancer immunotherapy[12,14].

In our laboratory, much research has been addressed to the study of AR antagonists belonging to different classes[15–26], including the 2-arylpyrazolo[4,3-*d*]pyrimidine derivatives[20,22,24,26] which display a broad range of affinity for the various AR subtypes, depending on the nature of the substituents at the 5- and 7-

CONTACT Vittoria Colotta vittoria.colotta@unifi.it Dipartimento di Neuroscienze, Psicologia, Area del Farmaco e Salute del Bambino, Sezione di Farmaceutica e Nutraceutica, Università di Firenze, Via Ugo Schiff, 6, 50019 Sesto Fiorentino, Italy; Stefano Moro stefano.moro@unipd.it Molecular Modeling Section (MMS), Dipartimento di Scienze del Farmaco, Università di Padova, via Marzolo 5, 35131 Padova, Italy

Supplemental data for this article can be accessed here

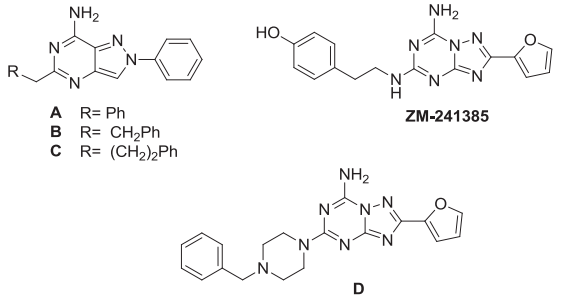

Figure 1. Previously reported pyrazolo[4,3-*d*]pyrimidines **A–C** and triazolotriazines ZM-241385 and **D**.

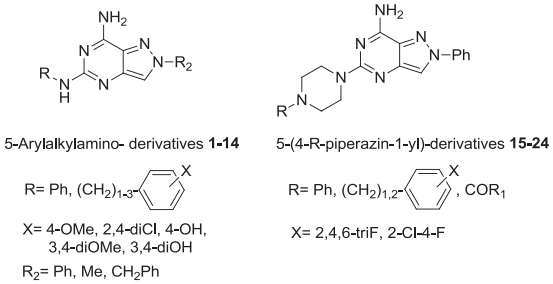

Figure 2. Herein reported pyrazolo[4,3-*d*]pyrimidine derivatives **1–24**.

positions of the bicyclic scaffold. One recent study aimed at targeting the A_1 and A_{2A} ARs highlighted that the presence of a free 7-amino group, combined with a benzyl or, even better, a 3-phenylpropyl chain at the 5-position (Figure 1, compounds **A** and **C**) shifted affinity toward these two AR subtypes[24].

Hence, to further explore the structural requirements for addressing affinity toward the A_1 and/or A_{2A} ARs, various aryl(alkyl)amino- and 4-substituted-piperazin-1-yl- moieties were appended at the 5-position of the scaffold (compounds **1–24**, Figure 2). These substituents were selected since they are a common feature of potent A_1 and/or A_{2A} AR antagonists structurally correlated to our pyrazolopyrimidine derivatives[12,27,28] (such as the triazolotriazines ZM-241385 and **D**, Figure 1). The pyrazolopyrimidines **1–24** were tested in binding assays to evaluate their affinity at cloned hA_1, hA_{2A} and hA_3 ARs, stably expressed in CHO cells. Compounds were also tested at the hA_{2B} receptor by measuring their inhibitory effects on NECA-stimulated cAMP levels in CHO cells.

A structure-based molecular modeling study was performed on the new derivatives to rationalize the experimental binding data from a molecular point of view, using molecular docking studies in tandem with Interaction Energy Fingerprints (IEFs) analysis.

Chemistry

The 7-amino-pyrazolo[4,3-*d*]pyrimidine derivatives **1–14**, bearing an arylalkylamino moiety at the 5-position, were obtained as displayed in Scheme 1.

Both the 1-phenyl (**26**) and 1-alkyl substituted pyrazoles (**27**, **28**) were synthesized from a common starting compound: the readily available 4-nitro-1H-pyrazole-3-carbonitrile **25**[26] which was a good substrate for both regioselective N-alkylation and N-arylation. The latter was achieved by a cross-coupling reaction with phenylboronic acid in the presence of cupric acetate and activated molecular sieves. The 1-phenyl-pyrazole derivative **26** was thus prepared with higher yield than those previously obtained in our laboratory through another synthetic pathway[22]. The 1-methyl- and 1-benzyl-pyrazoles **27** and **28** were prepared from compound **25** as already described[26]. The 4-nitropyrazolo-3-

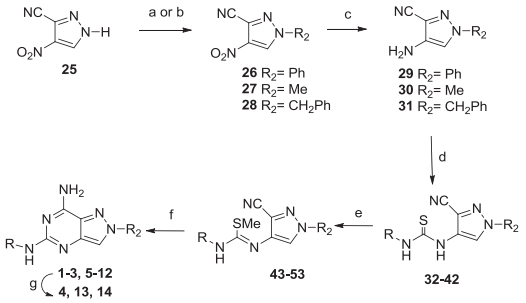

	R	R_2		R	R_2
32, 43, 1	Ph	Ph	**38, 49, 8**	Ph	Me
33, 44, 2	4-OMe-C_6H_4	Ph	**39, 50, 9**	Ph-CH_2	Me
34, 45, 3	2,4-diClC_6H_3	Ph	**40, 51, 10**	Ph-CH_2	CH_2Ph
4	4-OH-C_6H_4	Ph	**41, 52, 11**	4-OMe-C_6H_4-$(CH_2)_2$	Ph
35, 46, 5	Ph-CH_2	Ph	**42, 53, 12**	3,4-diOMe-C_6H_3-$(CH_2)_2$	Ph
36, 47, 6	Ph-$(CH_2)_2$	Ph	**13**	4-OH-C_6H_4-$(CH_2)_2$	Ph
37, 48, 7	Ph-$(CH_2)_3$	Ph	**14**	3,4-diOH-C_6H_3-$(CH_2)_2$	Ph

Scheme 1. Reagents and conditions: (a) Ph-$B(OH)_2$, $Cu(OAc)_2$, pyridine, CH_2Cl_2, 4 Å molecular sieves, room temperature; (b) MeI or $PhCH_2Br$, NaH, anhydrous THF, room temperature; (c) cyclohexene, Pd/C, 150 °C, mw; (d) R–N=C=S, DMF, room temperature; (e) 0.1 M aqueous NaOH, CH_3I, room temperature; (f) NH_4Cl, formamide, 110–150 °C mw; (g) compounds **2**, **11**, **12**, BBr_3, anhydrous CH_2Cl_2, room temperature or reflux.

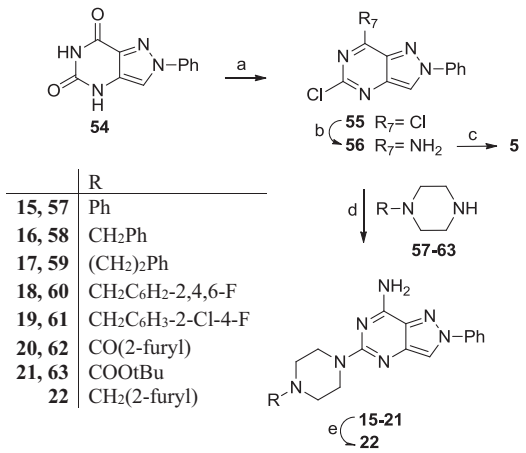

	R
15, 57	Ph
16, 58	CH_2Ph
17, 59	$(CH_2)_2Ph$
18, 60	$CH_2C_6H_2$-2,4,6-F
19, 61	$CH_2C_6H_3$-2-Cl-4-F
20, 62	CO(2-furyl)
21, 63	COOtBu
22	CH_2(2-furyl)

Scheme 2. Reagents and conditions: (a) N,N-dimethylaniline, $POCl_3$, 150 °C, mw; (b) 33% aqueous NH_3, 100 °C, mw; (c) benzylamine, ethyldiisopropylamine, tert-butanol, 200 °C, mw; (d) ethyldiisopropylamine, N-methylpyrrolidone, 130–150 °C, mw; (e) compound **20**, $LiAlH_4$, anhydrous THF, room temperature.

carbonitriles **26–28** were transformed into the corresponding 4-amino derivatives **29–31**[26] by reduction with cyclohexene and Pd/C, under microwave-assisted conditions. Reaction of compounds **29–31** with isothiocyanates in anhydrous DMF yielded the corresponding N-(1-substituted-3-cyano-pyrazol-4-yl)thiourea derivatives **32–42**. Phenyl-, 4-methoxyphenyl-, 2,4-dichlorophenyl- and benzyl-isothiocyanates were commercially available, the others were synthesized as previously reported, i.e. allowing the corresponding arylalkylamines to react with CS_2, in 30% hydrogen peroxide aqueous solution (phenylethyl-, phenylpropyl- and 3,4-dimethoxyphenyl-isothiocyanates)[29,30] or with thiophosgene and potassium carbonate, in CH_2Cl_2 under nitrogen atmosphere (4-methoxyphenylisothiocyanate)[31].

Compounds **32–42** were reacted with iodomethane in anhydrous DMF to give the corresponding S-methylisothiourea derivatives **43–53** which were cyclized to the desired 7-amino-5-arylalkylamino-pyrazolo[4,3-*d*]pyrimidines **1–3**, **5–12** by reaction with ammonium chloride in formamide, under microwave irradiation. The methoxy-substituted derivatives **2**, **11** and **12** were transformed into the corresponding hydroxy derivatives **4**, **13** and **14** by treatment with BBr_3 in anhydrous CH_2Cl_2.

The 7-amino-pyrazolo[4,3-*d*]pyrimidine derivatives **15**–**22**, bearing N-substituted-piperazine moieties at the 5-position, were obtained utilizing the synthetic route as described in Scheme 2.

Allowing the 1-phenylpyrazolo[4,3-*d*]pyrimidine-5,7-dione **54**[20] to react with phosphorus oxychloride and N,N-dimethylaniline under microwave irradiation, the 5,7-dichloro-derivative **55** was prepared, which was reacted with 33% aqueous ammonia solution under microwave irradiation at 100 °C to give the 7-amino-5-chloro-pyrazolopyrimidine **56** as the only regioisomer. The 7-amino structure of **56** was expected on the basis of the well-known different mobility of the two chlorine atoms in the pyrimidine ring, also condensed with diverse heterocyclic systems[32–34]. To confirm the structure, derivative **56** was treated with benzylamine in tert-butanol, in the presence of diisopropylethylamine, and the 7-amino-5-benzylaminopyrazole derivative **5**, already synthesized through the unambiguous synthesis as depicted in Scheme 1, was obtained. This reaction was carried out under prolonged microwave irradiation (about 1 h at 200 °C) but conversion of derivative **56** into **5** occurred with unsatisfactory yields. The ^{1}H NMR spectrum of the crude reaction (data not shown) displayed the presence of both the 5-benzylamino derivative **5** and the starting material **56** (ratio about 3.5:1), besides degradation compounds, thus indicating the poor reactivity of the C5 atom toward the primary benzyl ammine group. Instead, microwave-assisted reaction of the 5-chloro derivative **56** with the N-substituted piperazines **57**–**63**, in N-methylpyrrolidone and in the presence of diisopropylethylamine, proceeded to completion, thus giving the desired pyrazolopyrimidine derivatives **15**–**20** with good yields (48–85%). The piperazine derivatives **57, 58, 62** and **63** were commercially available, while derivatives **59** and **61** were prepared as previously described[35,36]. The piperazine derivative **60** was synthesized starting from the reductive alkylation of N-Boc-piperazine **63** with 2,4,6-trifluorobenzaldeyde and triacetoxy sodium borohydride. The obtained tert-butyl 4-(2,4,6-trifluorobenzyl)piperazine-1-carboxylate was hydrolyzed with trifluoroacetic acid to give the 1-(2,4,6-trifluorobenzyl)piperazine **60**, isolated as trifluoroacetate salt.

Reduction of the 2-furoyl carbonyl group of compound **20** with $LiAlH_4$ in anhydrous THF provided derivative **22**. Finally, the

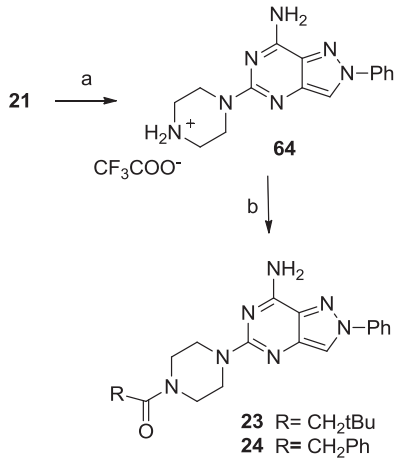

Scheme 3. Reagents and conditions: (a) CF_3COOH, CH_2Cl_2, reflux; (b) RCOCl, NEt_3, anhydrous THF, room temperature.

Table 1. Binding affinity at hA_1, hA_{2A} and hA_3 ARs and potencies at hA_{2B} ARs.

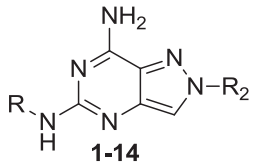
1-14

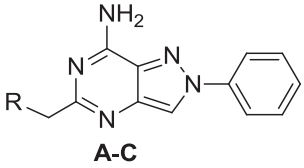
A-C

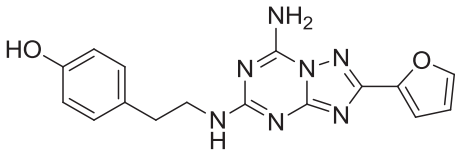
ZM-241385

			Binding experiments[a] K_i (nM) or I%			cAMP assays IC_{50} (nM) or I%
	R	R_2	hA_1[b]	hA_{2A}[c]	hA_3[d]	hA_{2B}[e]
1	Ph	Ph	67 ± 5	412 ± 37	13 ± 2	2%
2	4-OMe-C_6H_4	Ph	33%	8%	27 ± 3	1%
3	2,4-diClC_6H_3	Ph	1%	1%	61 ± 8	2%
4	4-OH-C_6H_4	Ph	481 ± 42	40%	8%	10%
5	Ph-CH_2	Ph	25 ± 3	123 ± 11	28 ± 3	2%
6	Ph-CH_2CH_2	Ph	11.5 ± 1.2	40%	38%	1%
7	Ph-$CH_2CH_2CH_2$	Ph	785 ± 72	29%	24%	1%
8	Ph	Me	1%	4%	1%	1%
9	Ph-CH_2	Me	9%	1%	20%	1%
10	Ph-CH_2	CH_2Ph	19%	1%	1%	1%
11	4-OMe-C_6H_4-CH_2CH_2	Ph	153 ± 11	26%	19%	1%
12	4-OH-C_6H_4-CH_2CH_2	Ph	27%	150 ± 14	1%	1%
13	3,4-diOMe-C_6H_3-$(CH_2)_2$	Ph	415 ± 39	189 ± 18	22%	17%
14	3,4-diOH-C_6H_3-$(CH_2)_2$	Ph	71 ± 6	238 ± 24	3%	1%
A[f]	Ph	–	150 ± 12	110 ± 10	39%	420 ± 38
B[f]	Ph-CH_2	–	15%	35%	17%	2%
C[f]	Ph-CH_2CH_2	–	5.31 ± 0.42	55 ± 5	12%	42%
ZM-241385[g]		–	714	1.6	743	75[h]

[a]K_i values are means ± SEM of four separate assays each performed in duplicate. Percentage of inhibition (I%) are determined at 1 μM concentration of the tested compounds.
[b]Displacement of specific [^{3}H]DPCPX competition binding assays to hA_1CHO cells.
[c]Displacement of specific [^{3}H]ZM241385 competition binding to hA_{2A}CHO cells.
[d]Displacement of specific [^{125}I]AB-MECA competition binding to hA_3CHO cells.
[e]cAMP experiments in hA_{2B}CHO cells, stimulated by 200 nM NECA. Percentage of inhibition (I%) are determined at 1 μM concentration of the tested compounds.
[f]Ref. 24.
[g]Ref. 5.
[h]K_i value obtained from binding experiments at recombinant hA_{2B}.

Table 2. Binding affinity at hA_1, hA_{2A} and hA_3 ARs and potencies at hA_{2B} ARs.

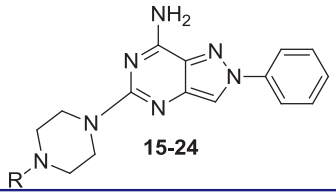

15-24

		Binding experiments[a] K_i (nM) or I%			cAMP assays I%
	R	hA_1[b]	hA_{2A}[c]	hA_3[d]	hA_{2B}[e]
15	Ph	647 ± 53	20%	20%	1%
16	CH_2Ph	162 ± 14	1%	1%	1%
17	$(CH_2)_2Ph$	518 ± 42	40%	40%	1%
18	$CH_2C_6H_2$-2,4,6-F	204 ± 18	34%	39%	1%
19	$CH_2C_6H_3$-2-Cl-4-F	193 ± 17	29%	1%	2%
20	CO-2-furyl	580 ± 47	16%	13%	2%
21	COOtBu	615 ± 49	33%	21%	1%
22	CH_2-2-furyl	92 ± 8	38%	5%	16%
23	$COCH_2tBu$	29%	2%	1%	2%
24	$COCH_2Ph$	429 ± 36	3%	1%	3%

[a]K_i values are means ± SEM of four separate assays each performed in duplicate. Percentage of inhibition (I%) are determined at 1 μM concentration of the tested compounds.
[b]Displacement of specific [^{3}H]DPCPX competition binding assays to hA_1CHO cells.
[c]Displacement of specific [^{3}H]ZM241385 competition binding to hA_{2A}CHO cells.
[d]Displacement of specific [^{125}I]AB-MECA competition binding to hA_3CHO cells.
[e]cAMP experiments in hA_{2B}CHO cells, stimulated by 200 nM NECA. Percentage of inhibition (I%) are determined at 1 μM concentration of the tested compounds.

pyrazolopyrimidines **23**–**24**, bearing an acyl moiety on the piperazine nitrogen, were synthesized as depicted in Scheme 3. Treatment of the N-Boc derivative **21** with trifluoroacetic acid furnished compound **64** which was reacted with suitable acyl chlorides, in the presence of triethylamine in anhydrous tetrahydrofuran, to provide the desired **23**–**24**.

Results and discussion

Structure–affinity relationship studies

The results of binding experiments and cAMP assays carried out on the new 5-substituted-pyrazolopyrimidines **1**–**14** and **15**–**24** are displayed, respectively, in Tables 1 and 2. Table 1 also includes the affinity data of the pyrazolopyrimidines **A**–**C** and of ZM-241385 reported as references.

As expected, the new derivatives **1**–**24** shared scarce or no affinities for the off-target hA_{2B} and hA_3 ARs, except the 5-anilino- and 5-benzylamino derivatives **1**–**3** and **5**, respectively which displayed nanomolar affinity for the hA_3 subtype (K_i = 13–61 nM). In particular, compounds **2** and **3** are worth noting, being also highly hA_3 selective.

Since the purpose of the work was to target hA_1 and hA_{2A} ARs, SAR discussion was focused on hA_1 and hA_{2A} binding data. In this respect, results of some interest have been obtained from the 5-arylalkylamino-pyrazolopyrimidines **1**–**14**. In fact, compound **12** showed both good affinity and the best selectivity for the hA_{2A} AR, while compounds **1**, **5**, **13** and **14** were able to bind both the hA_1 and hA_{2A} ARs. Moreover, a derivative having nanomolar affinity and high selectivity for the hA_1 AR subtype was identified (compound **6**).

The new 5-phenyl(alkyl)amino derivatives **1**, **5** and **6** were designed as analogs of our previously reported antagonists 5-phenyl(alkyl) derivatives **A**, **B** and **C**[24] whose methylene linker at the 5-position of the bicyclic core was replaced with an NH. This modification, suggested by the structure of potent A_{2A} antagonists bearing arylalkylamino moieties as key substituents[12], was thought to change the flexibility of the 5-lateral chain and, hopefully, to increase the affinity for the targeted ARs. Actually, the NH linker enhanced the hA_1 AR affinity (compare **1** and **5** to **A** and **B**, respectively) or maintained it in the nanomolar range (compare **6** to **C**). Instead, the hA_{2A} AR binding was ameliorated in one case, i.e. the 5-benzylamino derivative **5** which was more active than the corresponding phenylalkyl-derivative **B**.

Analyzing the hA_1 and hA_{2A} AR binding data of **1**–**6** in detail, it can be observed that 5-phenylamino derivative **1** binds to the hA_{2A} and hA_1 AR subtypes with scarce (K_i = 412 nM) and good affinity (K_i = 67 nM), respectively. Introduction of either a 4-methoxy group or 2,4-dichloro substituents on the 5-aniline moiety of **1** (compounds **2** and **3**) dropped affinity for hA_1 and hA_{2A} ARs. Instead, the presence of a 4-hydroxy residue (compound **4**) reduced the hA_{2A} affinity while conserving some ability to bind the hA_1 receptor (K_i = 481 nM). Homologation of the 5-phenylamino moiety (derivative **1**) to the 5-benzylamino group (derivative **5**) produced some improvement in the binding activity at both hA_1 (K_i = 25 nM) and hA_{2A} ARs (K_i = 123 nM). Quite unexpectedly, homologation of the alkyl chain of compound **5**, to obtain the 5-phenethylamino- and the 5-phenylpropylamino derivatives **6** and **7**, caused a drastic reduction of the hA_{2A} AR affinity and, in the former, it increased the hA_1 one, thus affording a selective hA_1 receptor ligand (K_i = 11.5 nM).

Replacement of the 2-phenyl group of derivatives **1** and **5** with a methyl residue, to give compounds **8** and **9**, was performed to verify whether a reduction in the volume of the molecule might permit a better accommodation inside the recognition site of the targeted hARs. This modification, instead, annulled the capability to bind the target hARs. The same detrimental effect was obtained when the 2-phenyl ring of **5** was replaced with the more flexible benzyl moiety (derivative **10**).

Insertion of the para hydroxy substituent on the 5-phenethylamino moiety of derivative **6**, to give compound **12**, was based on the structure of the well-known potent and selective hA_{2A} AR antagonist ZM-241385[5,12] (Figure 1). Accordingly, we also thought it would be interesting to evaluate the 3,4-dihydroxy substitution (compound **14**), as well as the 4-methoxy- and the 3,4-dimethoxy-substituents (derivatives **11** and **13**). As expected, the presence of the 4-hydroxy group was able to shift the affinity toward the hA_{2A} AR. In fact, the 4-hydroxy-substituted derivative **12** showed good hA_{2A} affinity (K_i = 150 nM) and the best selectivity among all the ligands reported here. In contrast, reversed selectivity was demonstrated by the 4-methoxy derivative **11**, which displayed good affinity for the hA_1 AR but not for the hA_{2A} subtype. Instead, the 3,4-dimethoxy substituted derivative **13** bound both hA_1 and hA_{2A} receptors and also the 3,4-dihydroxy derivative **14** showed quite good affinity for both the receptors, but especially for the hA_1 one.

Finally, to further explore the SARs in this class of AR ligands, various N-substituted piperazine moieties were appended at the 5-position (derivatives **15**–**24**, Table 2), in accordance with the structure of known potent and selective hA_{2A} AR antagonists[27,28].

In contrast to our expectations, none of the 5-(N^4-R-piperazin-1-yl) derivatives **15**–**24** were able to bind effectively the A_{2A} AR while they possessed affinity for the hA_1 AR subtype, falling in the high nanomolar range. The most active compounds proved to be **22** (K_i = 92 nM) and **16** (K_i = 162 nM) which bear, respectively, the (2-furyl)-methyl and 2-benzyl pendant on the N4-piperazine moiety. Introduction of halogen atoms on the benzyl moiety of **16** left almost unchanged the hA_1 AR affinity (compounds **18** and **19**)

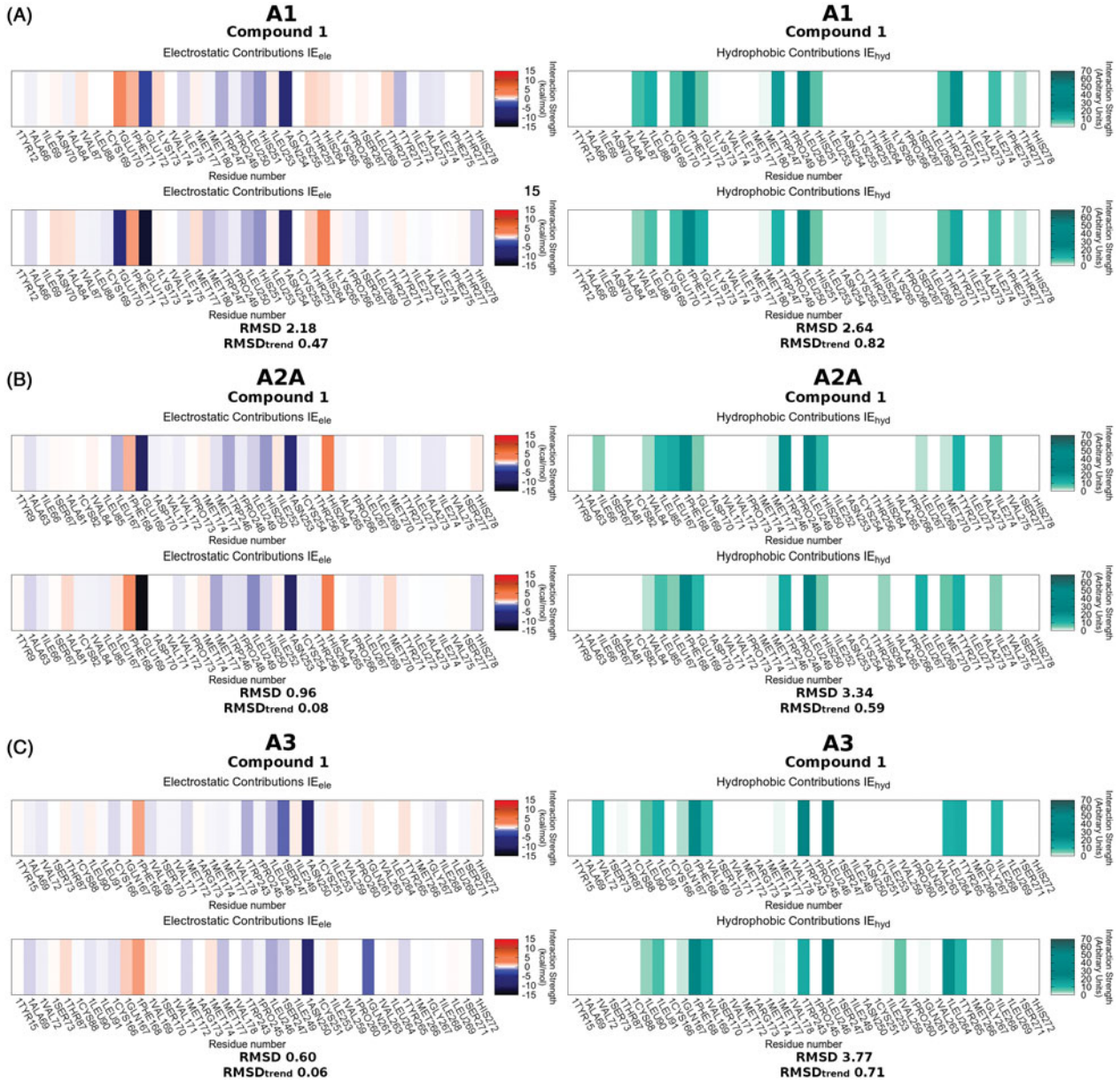

Figure 3. Interaction Energy Fingerprints (IEFs) comparison between compound 1 and compound ZM-241385 used as reference. Panels A, B and C report the comparison analysis for hA_1, hA_{2A} and hA_3 receptor subtypes, respectively. On the left side is shown the electrostatic contribution comparison, while on the right the hydrophobic one. In each subsection, the IEFs of compound **1** are shown above the IEFs of the reference ZM-241385.

while elongation of the benzyl chain decreased it (compound **17**). Also the other substituents evaluated on the piperazine ring, i.e. acyl moieties (derivatives **20**, **23**, **24**) and the tert-butoxycarbonyl group (derivative **21**) did not ameliorate the hA_1 AR affinities.

Molecular modeling studies

A structure-based molecular modeling study was conducted to rationalize the experimental binding data from a molecular point of view. Minor attention was devoted to the hA_{2B} AR subtype, since no significant binding affinity has been estimated for any of the compounds under investigation. Docking was performed on hA_1, hA_{2A} and hA_3 AR subtypes, and the resulting poses were evaluated according to the van der Waals and electrostatic interactions, as previously reported[37,38] and described in detail in the "Experimental" section. Positive electrostatic and van der Waals values were used as filters to reject unfavorable docking poses. One pose for each ligand was selected on the basis of the Interaction Energy Fingerprints (IEFs) and by visual inspection.

An overview of the most favorable poses of all compounds on hA_1, hA_{2A} and hA_3 ARs is reported in video SM1-SM2-SM3, included in Supplementary Material. The heat map depicted in the background reports the electrostatic and hydrophobic contributions of the residues mainly involved in binding ("ele" and "hyd" labels identify the major contribution type of the residue) by a colorimetric scale going from blue to green for negative to positive values. These crucial residues are mainly positioned on the superior half of TM6 and TM7 and EL2, and the overall binding modes of the compounds under examination are very consistent among them. Here, we describe in detail the poses of compound **1** as an example, because of its high binding affinity for all three AR subtypes taken into consideration ($K_i = 67$ nM for hA_1, $K_i = 412$ nM for hA_{2A} and $K_i = 13$ nM for hA_3).

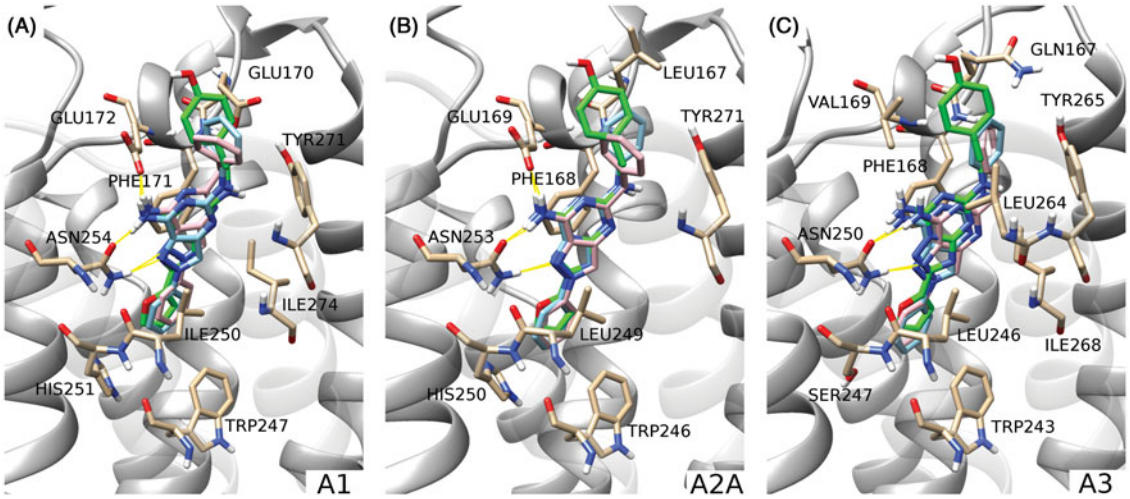

Figure 4. Comparison of the proposed binding mode of compound **1** (sky blue), compound **A** (pink), and reference pose of ZM-241385 (green) on hA_1, hA_{2A} and hA_3 subtype receptors (panels A, B and C, respectively). Protein residues mainly involved in binding are shown as sticks (tan). The zoom makes TM1 not visible, while TM6 and TM7 are rendered in a transparent manner to give a more clear visualization of the binding site.

With regard to the hA_1 AR, Glu172 (EL2) and Asn254 (6.55), represented by blue bars on electrostatic IEFs (Figure 3, panel A on the left), emerge as important residues for electrostatic contribution, together with a slight contribution of Trp247 (6.48) and His251 (6.52). Asn254 (6.55) and Glu172 (EL2) are engaged in a three hydrogen bond pattern with N1 of pyrazole and with the exocyclic amine group at position 7 of compound **1**, as shown in Figure 4, panel A. The aromatic pyrazolopyrimidine scaffold is involved in a π–π stacking interaction with Phe171 (EL2), which is one of the residues appearing to have the strongest hydrophobic interaction on the hydrophobic IEFs (green bars in Figure 3, panel A on the right). Val87 (3.32), Leu88 (3.33), Trp247 (6.48), Leu250 (6.51), Tyr271 (7.36) and Ile274 (7.39) are also involved in significant hydrophobic contacts, with Val87 (3.32), Leu88 (3.33), Trp247 (6.48) defining the bottom of the binding pocket.

The residues involved in binding at hA_{2A} AR are positioned equivalently to those just described for the hA_1 subtype. Glu169 (EL2) and Asn253 (6.55) are involved in hydrogen bonds and Phe168 (EL2) makes a π–π stacking interaction, as can be seen in Figure 4, panel B. Trp246 (6.48) and His250 (6.52), together with Glu169 and Asn253, give stabilizing electrostatic contributions to the binding of **1**, while Leu85 (3.33), Leu167 (EL2), Phe168 (EL2), Trp246 (6.48), Leu249 (6.51), Tyr271 (7.36) are interested by hydrophobic contacts (Figure 3, panel B).

The binding of compound **1** to the hA_3 subtype mainly engages Trp243 (6.48), Ser247 (6.52) and Asn250 (6.55) for electrostatic interactions, and Leu91 (3.33), Phe168 (EL2), Val169 (EL2), Trp243 (6.48), Leu246 (6.51), Leu264 (7.35), Tyr265 (7.36), Ile268 (7.39) for hydrophobic interactions, as can be seen in Figure 3, panel C. In this case only Asn250 can be involved in the hydrogen bond network (Figure 4, panel C), since in the A_3 AR the position equivalent to Glu172 of the hA_1 and Glu169 of the A_{2A} AR is occupied by Val169, which cannot establish a hydrogen bond with the amino group at position 5 of compound **1**.

Most of the poses resemble the conformation that ZM-241385 assumes in the binding site of the hA_{2A} AR crystal structure and of hA_1 and hA_3 AR models. The benzene ring at position 2 occupies the position of the furan ring of ZM-241385, the 7-amino-pyrazolopyrimidine scaffold is well superimposed on the reference 7-amino-triazolotriazine and the arylalkylamino group at position 5 points in the same direction as the para-hydroxyphenyl-ethylamino fragment. The similarity of the binding modes confirms the expectation provided by the IEFs comparison between **1** and ZM-241385 (Figure 3, panels A, B and C). To quantitatively compare the calculated IEFs profiles, two novel analyses have been proposed called RMSD and $RMSD_{trend}$ analysis (see the Experimental Section for more details). In the case of derivative **1** both RMSD and $RMSD_{trend}$ between electrostatic and hydrophobic IEFs on each hAR subtype are quite low. However, the electrostatic RMSD (2.18 kcal/mol) and the electrostatic $RMSD_{trend}$ (0.47 kcal/mol) for the hA_1 subtype are higher than the values observed for hA_{2A} and hA_3 ARs. This does not seem to fit with the low K_i (67 nM) for the hA_1 receptor; however, it appears that the major unfavorable contribution is provided by Glu170, which may probably be corrected by a slight rotation of the phenyl group of the compound.

Subsequently, we compared the binding behavior of compound **1** to that of its analog derivative **A** (K_i = 150 nM for hA_1, K_i = 110 nM for hA_{2A} and I% = 39 at 1 μM for hA_3), having a methylene instead of the NH linker at the 5-position. The IEFs comparison did not allow a complete rationalization of the different selectivity profiles of compounds **1** and **A** (Figure SM1). Electrostatic RMSD and $RMSD_{trend}$ values on the hA_3 receptor (1.10 and 0.18 kcal/mol, respectively) are higher than those of compound **1** (0.60 and 0.06 kcal/mol, respectively), in accordance with the lower potency of derivative **A** (I = 39% at 1 μM) compared with **1** (K_i = 13 nM). On the other hand, we have to honestly observe that also compound **A** presents higher RMSD and $RMSD_{trend}$ values (1.49 and 0.18 kcal/mol, respectively) on the hA_{2A} receptor as compared with compound **1** (0.96 and 0.08 kcal/mol, respectively), but in this case the affinity of the former (110 nM) is higher than that of the latter (412 nM). The result of the IEFs comparison is confirmed by the similarity of the binding modes of derivatives **1** and **A** at all receptor binding sites, as reported in Figure 4 (panels A, B and C). In this case docking is not sufficient to rationalize the difference in binding affinities. In fact, the mere examination of the final state of the binding process may not be sufficient to explain differences in the activity or selectivity profiles. The presence of water molecules and the entropic effect are only two among the pool of binding contributions that we are not taking into consideration during our docking simulations.

Similar considerations can be made observing the results of IEFs comparison for all the dataset compounds on the different AR subtypes (Figure 5). We would have expected to find blue and red rectangles associated with good and bad binders, respectively, but

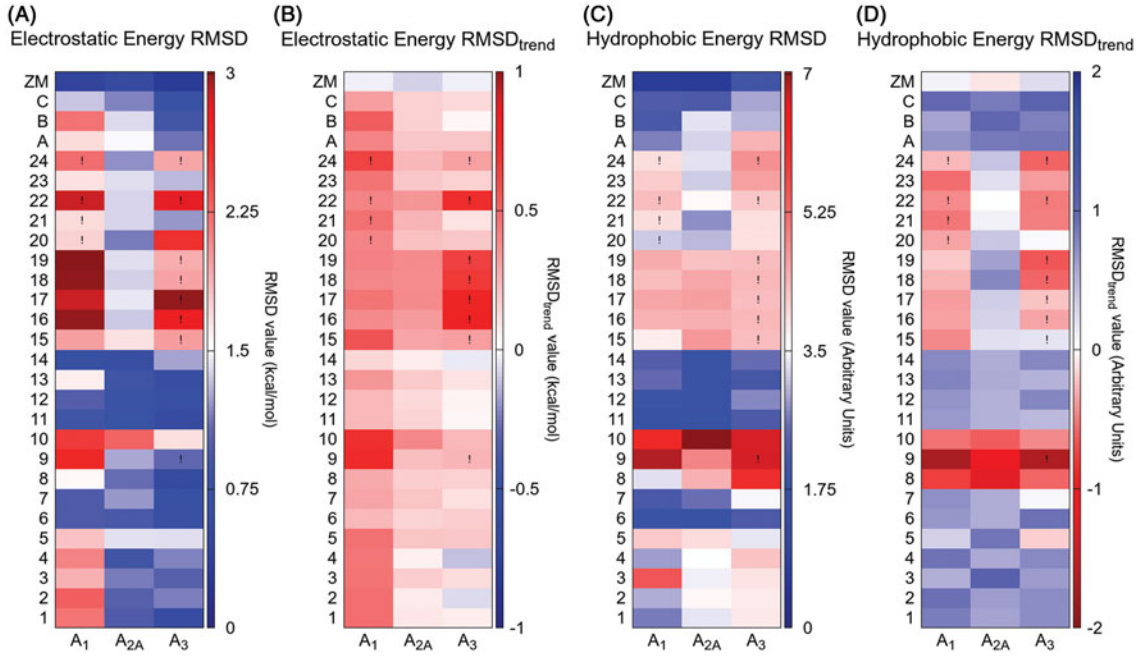

Figure 5. Results of the IEFs comparison between all compounds and reference compound ZM-241385. RMSDs and $RMSD_{trend}$ between electrostatic (panels A and B, respectively) and hydrophobic (panels C and D, respectively) Energy Fingerprints of each compound (*y*-axis) and reference ZM-241385 are reported for hA_1, hA_{2A} and hA_3 receptors (*x*-axis). A colorimetric scale going from blue to red represents favorable to unfavorable values. An exclamation point identifies those poses that have a positive van der Waals and/or electrostatic potential (and for which was not possible to select an alternative pose with negative values).

this prevision was not satisfied: a major similarity of the IEFs between the target and the reference compounds are not always related to good binding affinity of the ligand. However, an interesting example is provided by compounds **8**, **9** and **10**, which have no affinity for any of the receptors. Red rectangles cross horizontally almost the whole hydrophobic RMSD and $RMSD_{trend}$ table, meaning that there is a considerable loss in the binding hydrophobic contribution in comparison with the reference. As a control experiment, ZM-241385 has been docked into the three AR subtypes, the IEFs have been computed for the selected poses and compared with that of the reference pose of ZM241385: as expected, the electrostatic and hydrophobic RMSD and $RMSD_{trend}$ values are close to zero (Figure 5).

The 5-(N_4-R-piperazin-1-yl) compounds **15**–**24** are hA_1 AR selective. These derivatives find a steric hindrance in the hA_3 binding site and the van der Waals values of the selected poses are positive (as indicated by exclamation points in Figure 5). However, from the IEFs comparison analysis (Figure 5), we would have predicted a hA_{2A} versus hA_1 selectivity (blue versus red rectangles). In fact, while at the hA_{2A} binding site the predicted poses of these compounds behave like ZM-241385, at the hA_1 binding site they deviate a little from the reference position, losing some of the canonical interactions (Video SM1-SM2). Interestingly, this diversion results in a gain for compounds **16**, **17**, **18**, **19** and **22**: the protonated amine at position 4 of the piperazine moiety is involved in an ionic interaction with Glu170 (EL2), which is confirmed by a highly negative electrostatic contribution reported on the heat map in the background of Video SM1. The absence of a negatively charged residue at a position equivalent to Glu170 on hA_{2A} (Leu167) and hA_3 (Gln167) receptors may be associated with the hA_1 selectivity of these compounds.

Conclusion

The herein reported structural investigation was carried out to identify new antagonists targeting the hA_{2A} AR or both the hA_1/hA_{2A} ARs. Hence, various arylalkylamino- and 4-substituted-piperazin-1-yl- moieties were appended at the 5-position of the pyrazolo[4,3-d]pyrimidine scaffold. The 4-hydroxyphenylethylamino group was the most profitable, since the ZM-241385-based compound **12** showed both good hA_{2A} affinity (K_i = 150 nM) and the highest selectivity among all the ligands reported here. The 5-benzylamino moiety (compound **5**) achieved the best combined hA_{2A} (K_i = 123 nM) and hA_1 affinity (K_i = 25 nM) while the 5-phenethylamino pendant (compound **6**) afforded nanomolar affinity (K_i = 11 nM) and good selectivity for the hA_1 AR. The 5-(N^4-substituted-piperazin-1-yl) derivatives **15**–**24** were inactive at the hA_{2A} AR while the hA_1 affinities spanned the high nanomolar range. These outcomes provide new insights about the structural requirements of our pyrazolopyrimidine series for hA_{2A}- and hA_1-receptor ligand interaction. Nevertheless, the obtained results do not prompt us to synthesize further derivatives of this series featured by 5-arylalkyamino- and 5-piperazino- moieties.

A structure-based molecular modeling study was conducted to rationalize the experimental binding data from a molecular point of view using molecular docking studies in tandem with Interaction Energy Fingerprints (IEFs) analysis. Moreover, to quantitatively compare IEFs profiles and, consequently, to address the similarity of the binding modes of different compounds in different receptor subtypes, two novel analyses have been proposed, called RMSD and $RMSD_{trend}$ analyses. Even if, we are conscious that the simple inspection of the final state of the binding process may not be sufficient to explain differences in the activity or selectivity profiles, these novel tools can facilitate the mode of representation and interpretation of the docking data obtained by analyzing simultaneously several compounds against different receptor subtypes.

Experimental section

Chemistry

The microwave-assisted syntheses were performed using an Initiator EXP Microwave Biotage instrument (frequency of

irradiation: 2.45 GHz). Analytical silica gel plates (Merck F254), preparative silica gel plates (Merck F254, 2 mm) and silica gel 60 (Merck, 70–230 mesh) were used for analytical and preparative TLC, and for column chromatography, respectively. All melting points were determined on a Gallenkamp melting point apparatus and are uncorrected. Elemental analyses were performed with a Flash E1112 Thermofinnigan elemental analyzer for C, H, N and the results were within ±0.4% of the theoretical values. All final compounds revealed a purity not less than 95%. The IR spectra were recorded with a Perkin-Elmer Spectrum RX I spectrometer in Nujol mulls and are expressed in cm^{-1}. The ^1H NMR spectra were obtained with a Bruker Avance 400 MHz instrument. The chemical shifts are reported in δ (ppm) and are relative to the central peak of the solvent which was $CDCl_3$ or DMSO-d_6. The assignment of exchangeable protons (OH, and NH) was confirmed by addition of D_2O. The following abbreviations are used: s = singlet, d = doublet, t = triplet, m = multiplet, br = broad and ar = aromatic protons.

4-Nitro-1-phenyl-1H-pyrazole-3-carbonitrile 26[26]

The title compound was prepared with a different procedure from that previously described by us[26]. Briefly, phenylboronic acid (2.4 mmol), cupric acetate (1.8 mmol) and activated 4 Å molecular sieves (750 mg) were added to a solution of 4-nitro-1H-pyrazole-3-carbonitrile[26] (1.2 mmol) in anhydrous dichloromethane (8 mL) and pyridine (2.4 mmol). The mixture was stirred at room temperature, under air, in a loosely capped flask for two days, then it was diluted with chloroform (20–30 mL) and filtered through celite. The solution was extracted with 0.1 M HCl (15 ml for three times), the organic phase was anhydrified (Na_2SO_4) and evaporated at reduced pressure to give a solid which was collected by suction, washed with water and then cyclohexane and recrystallized. Yield 75%; m.p. 143–145 °C (cyclohexane/EtOH); ^1H NMR (DMSO-d_6) 7.54–7.63 (m, 3H, ar), 7.74–7.76 (m, 2H, ar), 8.71 (s, 1H, H-5).

General procedure for the synthesis of 3-substituted-1-(3-cyano-1-R_{2-1}H-pyrazol-4-yl)thioureas 32–42

The commercially available phenyl-, 4-methoxyphenyl-, 2,4-dichlorophenyl- and benzyl-isothiocyanates or the suitably synthesized phenethyl-[29], 4-methoxyphenethyl-[31], 3,4-dimethoxyphenethyl-[30], phenylpropyl-isothiocyanates[29] (1.97 mmol) were added to a solution of the 1-substituted-4-amino-pyrazole-3-carbonitriles **29–31**[26] (1.64 mmol) in anhydrous DMF (1.5 mL). The mixture was stirred at room temperature for 3–4 h (compounds **32**–**34**, **38**, **39**), for 16 h (compounds **35**, **40**, **42**) and for 24 h (compounds **36**, **37**, **41**).

The obtained dark slurry was treated with water (20 mL) and, in the case of compounds **33**–**35** and **39**, a solid precipitated which was collected by filtration. For derivatives **32**, **36**–**38**, **40–42**, the aqueous mixture was extracted with EtOAc (30 mL ×3). The combined organic extracts were anhydrified (Na_2SO_4) and the solvent evaporated at reduced pressure. The obtained solid was treated with Et_2O (5–10 mL) and isolated by filtration. Crude compound **42** was purified by column chromatography (eluent:cyclohexane/EtOAc/MeOH 6:4:1). Derivatives **32**, **38**–**40**, as well as **42**, were unstable upon recrystallization, hence they were used as such for the next step.

1-(3-Cyano-1-phenyl-1H-pyrazol-4-yl)-3-phenylthiourea 32 Yield 89%; ^1H NMR (DMSO-d_6) 7.19 (t, 1H, ar, J = 7.4 Hz), 7.36 (t, 2H, ar, J = 7.6 Hz), 7.46 (t, 1H, ar, J = 7.4 Hz), 7.51 (d, 2H, ar, J = 7.6 Hz), 7.58 (t, 2H, ar, J = 7.5 Hz), 7.88 (d, 2H, ar, J = 7.7 Hz), 8.97 (s, 1H, pyrazole proton), 9.68 (br s, 1H, NH), 10.04 (br, s, 1H, NH).

1-(3-Cyano-1-phenyl-1H-pyrazol-4-yl)-3-(4-methoxyphenyl)thiourea 33 Yield 95%; m.p. 165–167 °C (cyclohexane/EtOAc); ^1H NMR (DMSO-d_6) 3.75 (s, 3H, OCH_3), 6.95 (d, 2H, ar, J = 8.9 Hz), 7.33 (d, 2H, ar, J = 8.9 Hz), 7.46 (t, 1H, ar, J = 7.6 Hz), 7.58 (t, 2H, ar, J = 7.3 Hz), 7.89 (d, 2H, ar, J = 7.6 Hz), 8.95 (s, 1H, pyrazole proton), 9.56 (br s, 1H, NH), 9.89 (br s, 1H, NH). Anal. Calc. for $C_{18}H_{15}N_5OS$.

1-(3-Cyano-1-phenyl-1H-pyrazol-4-yl)-3-(2,4-dichlorophenyl)thiourea 34 Yield 98%; m.p. 166–169 °C (cyclohexane/EtOAc); ^1H NMR (DMSO-d_6) 7.44–7.60 (m, 5H, ar), 7.80 (s, 1H, ar), 7.96 (d, 2H, ar, J = 7.9 Hz), 9.02 (s, 1H, pyrazole proton), 9.82 (br s, 1H, NH), 9.98 (br s, 1H, NH). Anal. Calc. for $C_{17}H_{11}Cl_2N_5S$.

1-Benzyl-3-(3-cyano-1-phenyl-1H-pyrazol-4-yl)thiourea 35 Yield 74%; m.p. 180–183 °C (EtOH). ^1H NMR (DMSO-d_6) 4.75 (d, 2H, CH_2, J = 4.6 Hz), 7.26–7.34 (m, 5H, ar), 7.45 (t, 1H, ar, J = 7.3 Hz), 7.57 (t, 2H, ar, J = 7.4 Hz), 7.87 (d, 2H, ar, J = 8.1 Hz), 8.49 (br s, 1H, NH), 8.99 (s, 1H, H-5), 9.55 (br s, 1H, NH). Anal. Calc. for $C_{18}H_{15}N_5S$.

1-Phenylethyl-3-(3-cyano-1-phenyl-1H-pyrazol-4-yl)thiourea 36 Yield 55%; m.p. 161–164 °C (cyclohexane/EtOAc). ^1H NMR (DMSO-d_6) 2.88 (t, 2H, CH_2, J =7.5 Hz), 3.69–3.70 (m, 2H, CH_2), 7.23–7.34 (m, 5H, ar), 7.46 (t, 1H, ar, J = 7.0 Hz), 7.58 (t, 2H, ar, J = 7.7 Hz), 7.89 (d, 2H, ar, J = 7.7 Hz), 8.09 (br s, 1H, NH), 8.91 (s, 1H, pyrazole proton), 9.50 (s, 1H, NH). Anal. Calc. for $C_{19}H_{17}N_5S$.

1-(3-Cyano-1-phenyl-1H-pyrazol-4-yl)-3-phenylpropylthiourea 37 Yield 57%; m.p. 133–136 °C (cyclohexane/EtOAc). ^1H NMR (DMSO-d_6) 1.82–1.90 (m, 2H, CH_2), 2.63 (t, 2H, CH_2, J = 7.3 Hz), 3.49–3.50 (m, 2H, CH_2), 7.17–7.31 (m, 5H, ar), 7.45 (t, 1H, ar, J = 7.4 Hz), 7.57 (t, 2H, ar, J = 7.8 Hz), 7.88 (d, 2H, ar, J = 7.9 Hz), 8.09 (br s, 1H, NH), 8.95 (s, 1H, pyrazole proton), 9.42 (s, 1H, NH). Anal. Calc. for $C_{20}H_{19}N_5S$.

1-(3-Cyano-1-methyl-1H-pyrazol-4-yl)-3-phenylthiourea 38 Yield 45%; ^1H NMR (DMSO-d_6) 3.92 (s, 3H, CH_3), 7.17 (t, 1H, ar, J = 7.3 Hz), 7.36 (t, 2H, ar, J = 7.8 Hz), 7.48 (d, 2H, ar, J = 7.7 Hz), 7.95 (s, 1H, pyrazole proton), 8.39 (br s, 1H, NH), 12.11 (br s, 1H, NH).

1-Benzyl-3-(3-cyano-1-methyl-1H-pyrazol-4-yl)thiourea 39 Yield 56%; ^1H NMR (DMSO-d_6) 3.95 (s, 3H, CH_3), 5.84 (br s, 2H, CH_2), 7.19–7.39 (m, 5H, ar), 7.70 (s, 1H, pyrazole proton), 8.39 (br s, 1H, NH), 9.47 (br s, 1H, NH).

1-Benzyl-3-(1-benzyl-3-cyano-1H-pyrazol-4-yl)thiourea 40 Yield 50%; ^1H NMR (DMSO-d_6) 4.71 (d, 2H, CH_2, J = 4.5 Hz), 5.40 (s, 2H, CH_2), 7.26–7.40 (m, 10H, ar), 8.44 (br s, 1H, NH); 8.51 (s, 1H, pyrazole proton), 9.47 (s, 1H, NH).

1-(3-Cyano-1-phenyl-1H-pyrazol-4-yl)-3-(4-methoxyphenylethyl)thiourea 41 Yield 62%; m.p. 260–262 °C (cyclohexane/EtOAc). ^1H NMR (DMSO-d_6) 2.81 (t, 2H, CH_2, J =7.2 Hz), 3.65–3.67 (m, 2H, CH_2), 3.72 (s, 3H, CH_3), 6.88 (d, 2H, ar, J = 8.9 Hz), 7.17 (d, 2H, ar, J = 8.9 Hz), 7.46 (t, 1H, ar, J = 7.0 Hz), 7.58 (t, 2H, ar, J = 7.7 Hz), 7.87

(d, 2H, ar, $J = 7.7$ Hz), 8.05 (br s, 1H, NH), 8.91 (s, 1H, pyrazole proton), 9.48 (s, 1H, NH). Anal. Calc. for $C_{20}H_{19}N_5OS$.

1-(3-Cyano-1-phenyl-1H-pyrazol-4-yl)-3-[2-(3,4-dimethoxyphenyl)ethyl]thiourea 42 Yield 55%; ^{1}H NMR (DMSO-d_6) 2.81 (t, 2H, CH_2, $J = 7.2$ Hz), 3.69–3.72 (m, 5H, $OCH_3 + CH_2$), 3.75 (s, 3H, OCH_3), 6.76 (d, 1H, ar, $J = 8.1$ Hz), 6.84 (s, 1H, ar), 6.89 (d, 1H, ar, $J = 8.2$ Hz), 7.46 (t, 1H, ar, $J = 7.2$ Hz), 7.58 (t, 2H, ar, $J = 7.1$ Hz), 7.86 (d, 2H, ar, $J = 8.0$ Hz), 8.04 (br s, 1H, NH), 8.91 (s, 1H, pyrazole proton), 9.48 (br s, 1H, NH). Anal. Calc. for $C_{21}H_{21}N_5O_2S$.

General procedure for the synthesis of S-methylisothiourea derivatives 43–53

A mixture of the suitable thiourea derivatives **32**–**42** (0.92 mmol) and iodomethane (3.69 mmol) in 0.1 N NaOH solution (11.8 mL) was stirred at room temperature until the disappearance of the starting material (12–24 h). Then, glacial acetic acid was added until pH 6. The solid which precipitated was collected by filtration and dried, except compounds **46** and **51** which were isolated from the reaction mixture by extraction with EtOAc (30 mL ×3). Evaporation of the anhydrified (Na_2SO_4) organic phase gave a solid which was collected by filtration. These S-methylisothiourea derivatives were unstable upon recrystallization, thus they were used for the next step without further purification. It was observed that derivatives **43**–**45** and **51** exist in two tautomeric forms in DMSO solution. In fact, in their ^{1}H NMR spectra there are two signals assignable to the SCH_3 and to the pyrazole proton. Compounds **44** and **51** also display, two signals assignable to the OCH_3 and SCH_3 substituents, respectively (see below for details).

N-(3-Cyano-1-phenylpyrazolo-4-yl)-N′-phenyl-S-methylisothiourea 43 Yield 86%; ^{1}H NMR (DMSO-d_6) mixture of two tautomers (ratio about 1:2.7) 2.35 (s, SCH_3), 2.38 (s, SCH_3), 7.30–7.31 (m, ar), 7.42–7.60 (m, ar +2 NH), 7.98 (d, ar, $J = 8.0$ Hz), 8.89 (s, pyrazole proton), 8.93 (s, pyrazole proton).

N-(3-Cyano-1-phenylpyrazolo-4-yl)-N′-4-methoxyphenyl-S-methylisothiourea 44 Yield 98%; ^{1}H NMR (DMSO-d_6) mixture of two tautomers (ratio about 1:3.2) 2.41 (s, SCH_3), 2.43 (s, SCH_3), 3.86 (s, OCH_3), 3.88 (s, OCH_3), 7.41–7.72 (m, ar), 7.96–8.01 (m, ar), 8.93 (s, pyrazole proton), 9.01 (br s, pyrazole proton + NH).

N′-2,4-Dichlorophenyl-N-(3-cyano-1-phenylpyrazolo-4-yl)-S-methylisothiourea 45 Yield 95%; ^{1}H NMR (DMSO-d_6) mixture of two tautomers (ratio about 1:3.6) 2.36 (s, SCH_3), 2.42 (s, SCH_3), 7.09–7.70 (m, ar), 8.00–8.16 (m, ar + NH), 9.00 (s, pyrazole proton), 9.18 (s, pyrazole proton).

N′-Benzyl-N-(3-cyano-1-phenylpyrazolo-4-yl)-S-methylisothiourea 46 Yield 98%; ^{1}H NMR (DMSO-d_6) 2.48 (s, 3H, SCH_3), 5.47 (br s, 2H, CH_2) 7.24–7.34 (m, 5H, ar), 7.44 (t, 1H, ar, $J = 7.3$ Hz), 7.57 (t, 2H, ar, $J = 7.6$ Hz), 7.97 (d, 2H, ar, $J = 8.0$ Hz), 8.13 (br s, 1H, NH), 8.80 (s, 1H, pyrazole proton).

N-(3-Cyano-1-phenylpyrazolo-4-yl)-N′-phenylethyl-S-methylisothiourea 47 Yield 86%; ^{1}H NMR (DMSO-d_6) 2.56 (s, 3H, CH_3), 3.04 (t, 2H, CH_2, $J = 7.1$ Hz), 4.33 (t, 2H, CH_2, $J = 7.1$ Hz), 7.25–7.41 (m, 5H, ar), 7.43 (t, 1H, ar, $J = 9.2$ Hz), 7.57 (t, 2H, ar, $J = 9.2$ Hz), 7.98 (d, 2H, ar, $J = 9.2$ Hz), 8.14 (s, 1H, NH), 8.86 (s, 1H, pyrazole proton).

N-(3-Cyano-1-phenylpyrazolo-4-yl)-N′-phenylpropyl-S-methylisothiourea 48 Yield 86%; ^{1}H NMR (DMSO-d_6) 2.03–2.05 (m, 2H, CH_2), 2.51 (s, 3H, CH_3), 2.71 (t, 2H, CH_2, $J = 7.4$ Hz), 4.16 (t, 2H, CH_2, $J = 7.4$ Hz), 7.21 (t, 1H, ar, $J = 9.0$ Hz), 7.27–7.32 (m, 4H, ar), 7.42 (t, 1H, ar, $J = 9.0$ Hz), 7.56 (t, 2H, ar, $J = 9.0$ Hz), 7.96 (d, 2H, ar, $J = 9.0$ Hz), 8.03 (s, 1H, NH), 8.83 (s, 1H, pyrazole proton).

N-(3-Cyano-1-methylpyrazolo-4yl)-N′-phenyl-S-methylisothiourea 49 Yield 87%; ^{1}H NMR (DMSO-d_6) 2.23 (s, 3H, SCH_3), 3.39 (s, 3H, CH_3), 7.33–7.35 (m, 2H, ar), 7.52–7.60 (m, 3H, ar), 8.07 (s, 1H, pyrazole proton).

N′-Benzyl-N-(3-cyano-1-methylpyrazolo-4-yl)-S-methylisothiourea 50 Yield 84%; ^{1}H NMR (DMSO-d_6) 2.43 (s, 3H, SCH_3), 3.99 (s, 3H, CH_3), 5.42 (br s, 2H, CH_2), 7.20–7.30 (m, 5H, ar), 7.75 (s, 1H, NH), 8.05 (s, 1H, pyrazole proton).

N′-Benzyl-N-(3-cyano-1-benzylpyrazolo-4-yl)-S-methylisothiourea 51 Yield 81%; ^{1}H NMR (DMSO-d_6) mixture of two tautomers (ratio about 1:6) 2.40 (s, SCH_3) 2.43 (s, SCH_3), 5.41 (br s, CH_2), 5.48 (s, CH_2), 7.14–7.39 (m, ar), 7.81 (br s, NH), 8.25 (s, pyrazole proton), 8.17 (s, pyrazole proton).

N′-4-Methoxyphenylethyl-N-(3-cyano-1-phenylpyrazolo-4-yl)-S-methylisothiourea 52 Yield 86%; ^{1}H NMR (DMSO-d_6) 2.56 (s, 3H, SCH_3), 2.97 (t, 2H, CH_2, $J = 7.3$ Hz), 3.75 (s, 3H, OCH_3), 4.29 (t, 2H, CH_2, $J = 7.3$ Hz), 6.91 (d, 2H, ar, $J = 9.5$ Hz), 7.24 (d, 2H, ar, $J = 9.5$ Hz), 7.43 (t, 1H, ar, $J = 9.5$ Hz), 7.57 (t, 2H, ar, $J = 9.3$ Hz), 7.98 (d, 2H, ar, $J = 9.3$ Hz), 8.11 (s, 1H, NH), 8.85 (s, 1H, pyrazole proton).

N′-3,4-Dimethoxyphenylethyl-N-(3-cyano-1-phenylpyrazolo-4-yl)-S-methylisothiourea 53 Yield 73%; ^{1}H NMR (DMSO-d_6) 2.58 (s, 3H, SCH_3), 2.98 (t, 2H, CH_2, $J = 8.5$ Hz), 3.73 (s, 3H, OCH_3), 3.76 (s, 3H, OCH_3), 4.34 (t, 2H, CH_2, $J = 7.2$ Hz), 6.83–6.93 (m, 4H, 3 ar + NH), 7.45 (t, 1H, ar, $J = 7.3$ Hz), 7.59 (t, 2H, ar, $J = 7.8$ Hz), 7.99 (d, 2H, ar, $J = 8.3$ Hz), 8.95 (s, 1H, pyrazole proton).

General procedure for the synthesis of 5-aryl(alkyl)amino-7-amino-2H-pyrazolo[4,3-d]pyrimidine derivatives 1–3, 5–12

A mixture of the suitable S-methylisothioureas **43**–**53** (1 mmol) and NH_4Cl (20 mmol) in formamide (2 mL) was microwave irradiated at 110 °C for 20 min (compounds **9**, **10**), at 130 °C for 40 min (compound **12**) and for 2 h (compounds **2**, **3**), at 150 °C for 15 min (compounds **1**, **5**, **8**) and for 20 min (compounds **6**, **7**, **11**). The suspension was then treated with $NaHCO_3$ saturated solution until pH 7 and the obtained solid was collected by filtration to give compounds **1**–**3**. To isolate derivatives **5**–**12**, the mixture was extracted with $CHCl_3$ (15 mL ×3), the organic phase was washed with water (15 mL ×2) and anhydrified (Na_2SO_4). Evaporation of the solvent at reduced pressure afforded a residue which was taken up with diethyl ether (2–3 mL) and collected by filtration. The crude derivatives were purified by recrystallization, except compounds **1**, **6, 7, 10, 11** which were first purified by column chromatography or preparative TLC (see below for details).

7-Amino-5-phenylamino-2-phenyl-2H-pyrazolo[4,3-d]pyrimidine 1 Purified by column chromatography (Et_2O/cyclohexane/EtOAc 3:1:1). Yield 66%; m.p. 252–254 °C (EtOH). ^{1}H NMR (DMSO-d_6) 6.86

(t, 1H, ar, $J = 7.3$ Hz), 7.23 (t, 2H, ar, $J = 7.6$ Hz), 7.41–7.45 (m, 3H, 1 ar + NH_2), 7.58 (t, 2H, ar, $J = 7.6$ Hz), 7.90 (d, 2H, ar, $J = 8.5$ Hz), 8.03 (d, 2H, ar, $J = 8.5$ Hz), 8.74 (s, 1H, H-3), 8.76 (br s, 1H, NH). Anal. Calc. for $C_{17}H_{14}N_6$.

7-Amino-5-(4-methoxyphenyl)amino-2-phenyl-2H-pyrazolo[4,3-d]pyrimidine 2 Yield 62%; m.p. 253–255 °C (cyclohexane/EtOAc); ^{1}H NMR (DMSO-d_6) 3.82 (s, 3H, OCH_3), 6.84 (d, 2H, ar, $J = 8.9$ Hz), 7.45–7.40 (m, 3H, 1 ar + NH_2), 7.58 (t, 2H, ar, $J = 7.7$ Hz), 7.75 (d, 2H, $J = 8.9$ Hz), 8.02 (d, 2H, ar, $J = 8.2$ Hz), 8.57 (s, 1H, NH), 8.68 (s, 1H, H-3). Anal. Calc. for $C_{18}H_{16}N_6O$.

7-Amino-5–(2,4-dichlorophenyl)amino-2-phenyl-2H-pyrazolo[4,3-d]pyrimidine 3 Yield 58%; m.p. 251–252 °C (cyclohexane/EtOAc); ^{1}H NMR (DMSO-d_6) 7.40–7.48 (m, 3H, 2 ar + NH), 7.54 (s, 1H, ar), 7.53–7.61 (m, 2H, ar), 7.61–7.79 (br s, 2H, NH_2), 8.02 (d, 2H, $J = 7.9$ Hz), 8.67 (d, 1H, $J = 8.9$ Hz), 8.82 (s, 1H, H-3). Anal. Calc. for $C_{17}H_{12}Cl_2N_6$.

7-Amino-5-benzylamino-2-phenyl-2H-pyrazolo[4,3-d]pyrimidine 5 Purified by preparative TLC (Et_2O/cyclohexane/EtOAc 3:1:1). Yield 60%; m.p. 143–145 °C (cyclohexane/EtOAc). ^{1}H NMR (DMSO-d_6) 4.49 (d, 2H, CH_2, $J = 6.3$ Hz), 6.71 (t, 1H, NH, $J = 6.3$ Hz), 7.18 (t, 1H, ar, $J = 7.1$ Hz), 7.26–7.34 (m, 6H, 4 ar + NH_2), 7.39 (t, 1H, ar, $J = 7.4$ Hz), 7.55 (t, 2H, ar, $J = 7.5$ Hz), 7.95 (d, 2H, ar, $J = 7.6$ Hz), 8.48 (s, 1H, H-3). Anal. Calc. for $C_{18}H_{16}N_6$.

7-Amino-5-(2-phenylethyl)amino-2-phenyl-2H-pyrazolo[4,3-d]pyrimidine 6 Purified by column chromatography (cyclohexane/EtOAc/MeOH 6:4:1). Yield 65%; m.p. 168–171 °C (cyclohexane/EtOAc). ^{1}H NMR (DMSO-d_6) 2.86 (t, 2H, CH_2, $J = 7.1$ Hz), 3.45–3.50 (m, 2H, CH_2), 6.12 (br s, 1H, NH), 7.18–7.32 (m, 7H, 5 ar + NH_2), 7.39 (t, 1H, ar, $J = 7.5$ Hz), 7.56 (t, 2H, ar, $J = 7.5$ Hz), 7.98 (d, 2H, ar, $J = 7.7$ Hz), 8.52 (s, 1H, H-3). Anal. Calc. for $C_{19}H_{18}N_6$.

7-Amino-5-(3-phenylpropyl)-2-phenyl-2H-pyrazolo[4,3-d]pyrimidines 7 Purified by column chromatography (eluent cyclohexane/EtOAc/MeOH 6:4:1). Yield 58%; m.p. 159–162 °C (EtOAc). ^{1}H NMR (DMSO-d_6) 1.83–1.86 (m, 2H, CH_2), 2.64 (t, 2H, CH_2, $J = 7.4$ Hz), 3.27 (m, 2H, CH_2), 6.20 (br s, 1H, NH), 7.19–7.30 (m, 7H, 5 ar + NH_2), 7.40 (t, 1H, ar, $J = 9.0$ Hz), 7.56 (t, 2H, ar, $J = 7.6$ Hz), 7.97 (d, 2H, ar, $J = 7.9$ Hz), 8.50 (s, 1H, H-3). Anal. Calc. for $C_{20}H_{20}N_6$.

7-Amino-2-methyl-5-phenylamino-2H-pyrazolo[4,3-d]pyrimidine 8 Yield 42%; m.p. 252–254 °C (EtOH). ^{1}H NMR (DMSO-d_6) 4.05 (s, 3H, Me), 6.84 (t, 1H, ar, $J = 7.2$ Hz), 7.19–7.21 (m, 4H, 2 ar + NH_2), 7.75 (d, 2H, ar, $J = 7.2$ Hz), 7.87 (s, 1H, H-3), 8.62 (br s, 1H, NH). Anal. Calc. for $C_{12}H_{12}N_6$.

7-Amino-5-benzylamino-2-methyl-2H-pyrazolo[4,3-d]pyrimidine 9 Yield 80%; m.p. 213–214 °C (EtOH); ^{1}H NMR (DMSO-d_6) 3.98 (s, 3H, CH_3), 4.45 (d, 2H, CH_2, $J = 6.4$ Hz), 6.47 (br s, 1H, NH), 7.05 (br s, 2H, NH_2), 7.16–7.32 (m, 5H, ar), 7.70 (s, 1H, H-3). IR: 3326, 3179, 1658. Anal. Calc. For $C_{13}H_{14}N_6$.

7-Amino-2-benzyl-5-benzylamino-2H-pyrazolo[4,3-d]pyrimidine 10 Yield 40%; m.p. 174–175 °C (cyclohexane/EtOAc). ^{1}H NMR (DMSO-d_6) 4.45 (d, 2H, CH_2, $J = 6.3$ Hz), 5.45 (s, 2H, CH_2), 6.58 (br s, 1H, NH), 7.11 (br s, 2H, NH_2), 7.15–7.36 (m, 10H, ar), 7.87 (s, 1H, H-3). Anal. Calc. for $C_{19}H_{18}N_6$.

7-Amino-5-[2–(4-methoxyphenyl)ethyl]amino-2-phenyl-2H-pyrazolo[4,3-d]pyrimidine 11 Purified by column chromatography (cyclohexane/EtOAc/MeOH 6:4:1), Yield 58%; m.p. 142–145 °C (cyclohexane/EtOAc). ^{1}H NMR (DMSO-d_6) 2.73 (t, 2H, CH_2, $J = 7.3$ Hz), 3.38–3.41 (m, 2H, CH_2), 3.73 (s, 3H, OCH_3), 6.03 (br s, 1H, NH), 6.69 (d, 2H, ar, $J = 8.9$ Hz), 7.04 (d, 2H, ar, $J = 8.9$ Hz), 7.22 (br s, 2H, NH_2), 7.41 (t, 1H, ar, $J = 7.3$ Hz), 7.57 (t, 2H, ar, $J = 7.6$ Hz), 7.98 (d, 2H, ar, $J = 7.9$ Hz), 8.51 (s, 1H, H-3). Anal. Calc. for $C_{20}H_{20}N_6O$.

7-Amino-5-[2-(3,4-dimethoxyphenyl)ethyl]amino-2-phenyl-2H-pyrazolo[4,3-d]pyrimidine 12 Purified by preparative TLC (cyclohexane/EtOAc/MeOH 6:4:1). Yield 45%; m.p. 100–102 °C (H_2O/MeOH). ^{1}H NMR (DMSO-d_6) 2.79 (t, 2H, CH_2, $J = 7.2$ Hz), 3.43–3.48 (m, 2H, CH_2), 3.72 (s, 3H, OCH_3), 3.74 (s, 3H, OCH_3), 6.10 (br s, 1H, NH), 6.75 (d, 1H, ar, $J = 6.5$ Hz), 6.84–6.87 (m, 2H, ar), 7.27 (br s, 2H, NH_2), 7.39 (t, 1H, ar, $J = 7.2$ Hz), 7.56 (t, 2H, ar, $J = 7.7$ Hz), 7.97 (d, 2H, ar, $J = 7.8$ Hz), 8.51 (s, 1H, H-3). Anal. Calc. for $C_{21}H_{22}N_6O_2$.

General procedure for the synthesis of the pyrazolo[4,3-d]pyrimidine-7-amine derivatives 4, 13 and 14

To a suspension of the methoxy-substituted pyrazolopyrimidine derivatives **2**, **11** and **12** (1.02 mmol) in anhydrous CH_2Cl_2 (20 mL), a 1 M BBr_3 solution (2.60 mL for **2**, **11** and 5.2 mL for **12**) in CH_2Cl_2 was added at 0 °C, under nitrogen atmosphere. The mixture was stirred at room temperature for 20–24 h (compounds **4**, **13**) or 16 h (compound **14**), then was diluted with water (10 mL) and neutralized with $NaHCO_3$ saturated solution. The organic solvent was removed under reduced pressure and the obtained precipitate was collected by filtration and recrystallized. The crude derivative **4** was first purified by column chromatography (eluent $CHCl_3$/MeOH 9:1) and then recrystallized.

7-Amino-5-(4-hydroxyphenyl)amino-2-phenyl-2H-pyrazolo[4,3-d]pyrimidine 4 Yield 67%; m.p. 223–225 °C (EtOAc/cyclohexane); ^{1}H NMR (DMSO-d_6) 6.65 (d, 2H, ar, $J = 8.8$ Hz), 7.30–7.45 (m, 3H, 2 ar + NH_2), 7.57 (t, 2H, ar, $J = 7.6$ Hz), 7.63 (d, 2H, ar, $J = 8.8$ Hz), 8.01 (d, 2H, ar, $J = 8.3$ Hz), 8.41 (s, 1H, NH), 8.65 (s, 1H, H-3), 8.85 (s, 1H, OH). Anal. Calc. for $C_{17}H_{14}N_6O$.

7-Amino-5-(4-hydroxyphenethyl)amino-2-phenyl-2H-pyrazolo[4,3-d]pyrimidine 13 Yield 89%; m.p. 241–244 °C (EtOAc/EtOH). ^{1}H NMR (DMSO-d_6) 2.73 (t, 2H, CH_2, $J = 7.3$ Hz), 3.38–3.40 (m, 2H, CH_2), 6.03 (br s, 1H, NH), 6.68 (d, 2H, ar, $J = 8.3$ Hz), 7.04 (d, 2H, ar, $J = 8.3$ Hz), 7.22 (br s, 2H, NH_2), 7.41 (t, 1H, ar, $J = 7.4$ Hz), 7.56 (t, 2H, ar, $J = 7.7$ Hz), 7.97 (d, 2H, ar, $J = 7.8$ Hz), 8.51 (s, 1H, H-3), 9.14 (s, 1H, OH). Anal. Calc. for $C_{19}H_{18}N_6O$.

7-Amino-5-(3,4-dihydroxyphenethyl)amino-2-phenyl-2H-pyrazolo[4,3-d]pyrimidine 14 Yield 50%; m.p. 242–243 °C (EtOH). ^{1}H NMR (DMSO-d_6) 2.65 (t, 2H, CH_2, $J = 7.1$ Hz), 3.37–3.41 (m, 2H, CH_2), 6.03 (t, 1H, NH, $J = 5.8$ Hz), 6.59–6.47 (d, 1H, ar, $J = 8.0$ Hz), 6.63–6.66 (m, 2H, ar), 7.23 (br s, 2H, NH_2), 7.40 (t, 1H, ar, $J = 7.4$ Hz), 7.56 (t, 2H, ar, $J = 7.6$ Hz), 7.97 (d, 2H, ar, $J = 7.7$ Hz), 8.51 (s, 1H, H-3), 8.62 (br s, 1H, OH), 8.74 (br s, 1H, OH). Anal. Calc. for $C_{19}H_{18}N_6O_2$.

Synthesis of 5,7-dichloro-2-phenyl-2H-pyrazolo[4,3-d]pyrimidine 55

A suspension of the pyrazolopyrimidine-5,7-dione derivative **54**[20] (2 mmol) and N,N-dimethylaniline (3.95 mmol) in phosphorus

oxychloride (5 mL) was microwave irradiated at 150 °C for 20 min. The excess of phosphorus oxychloride was distilled off under reduced pressure and the residue was treated with water (about 5 – 10 mL). The crude product was collected by filtration and recrystallized. Yield 96%; m.p. 252–254 °C (EtOH). ^{1}H NMR (DMSO-d_6) 7.62 (t, 1H, ar, $J = 9.1$ Hz), 7.69 (t, 2H, ar, $J = 9.3$ Hz), 8.17 (d, 2H, ar, $J = 9.1$ Hz), 9.69 (s, 1H, H-3). Anal. Calc. for $C_{11}H_6N_4Cl_2$.

Synthesis of 7-amino-5-chloro-2-phenyl-2H-pyrazolo[4,3-d]pyrimidine 56

A suspension of the suitable 5,7-dichloropyrazolopyrimidine derivative **55** (1.72 mmol) in aqueous 33% ammonia solution (10 mL) was microwave irradiated at 100 °C for 30 min. The suspension was cooled at room temperature and the solid was collected by filtration and recrystallized. Yield 90%; m.p. 260–261 °C (2-ethoxyethanol). ^{1}H NMR (DMSO-d_6) 7.50 (t, 1H, ar, $J = 8.0$ Hz), 7.62 (t, 2H, ar, $J = 8.0$ Hz), 8.05 (d, 2H, ar, $J = 8.0$ Hz), 8.35 (br s, 1H, NH_2), 8.38 (br s, 1H, NH_2), 9.05 (s, 1H, H-3). Anal. Calc. for $C_{11}H_8ClN_5$.

General procedure for the synthesis of 5-(4-R-piperazin-1-yl)-substituted pyrazolo[4,3-d]pyrimidines 15–21

A mixture of the 5-chloro-pyrazolopyrimidine derivative **56** (0.41 mmol), the suitable N-substituted piperazine **57**–**63** (0.82 mmol) and ethyldiisopropylamine (0.49 mmol) in N-methylpyrrolidone (2 mL) was heated by microwave irradiation in the conditions described below for each compound. The obtained slurry was poured dropwise into water (50 mL) under vigorous stirring. The solid which precipitated was collected by filtration, purified by chromatography (column or preparative TLC, as reported below for each derivative) and then recrystallized, except derivative **16** which was directly recrystallized.

The not commercially available 1-substituted piperazines were prepared as reported below (**60**) or as previously described (**59**, **61**)[35,36].

7-Amino-2-phenyl-5-(4-phenylpiperazin-1-yl)-2H-pyrazolo[4,3-d]pyrimidine 15 The reaction mixture was microwave irradiated at 150 °C for 15 min. Column chromatography, eluent: acetonitrile. Yield 48%; m.p. 183–185 °C (cyclohexane/EtOAc). ^{1}H NMR (DMSO-d_6) 3.18–3.20 (m, 4H, piperazine protons), 3.80–3.85 (m, 4H, piperazine protons), 6.80 (t, 1H, ar, $J = 7.1$ Hz), 7.00 (d, 2H, ar, $J = 7.3$ Hz), 7.24 (t, 2H, ar, $J = 7.3$ Hz), 7.40–7.46 (m, 3H, 1 ar, $+NH_2$), 7.57 (t, 2H, ar, $J = 7.5$ Hz), 8.00 (d, 2H, ar, $J = 8.4$ Hz), 8.59 (s, 1H, H-3). Anal. Calc. for $C_{21}H_{21}N_7$.

7-Amino-5-(4-benzylpiperazin-1-yl)-2-phenyl-2H-pyrazolo[4,3-d]pyrimidine 16 The reaction mixture was microwave irradiated at 130 °C for 25 min. Yield 74%; m.p. 201–202 °C (diisopropyl ether/MeOH). ^{1}H NMR (DMSO-d_6) 2.39–2.42 (m, 4H, piperazine protons), 3.50 (s, 2H, CH_2), 3.67–3.71 (m, 4H, piperazine protons), 7.24–7.29 (m, 1H, ar), 7.33–7.35 (m, 4H, ar), 7.39–7.42 (m, 3H, 1 ar + NH_2), 7.56 (t, 2H, ar, $J = 7.6$ Hz), 7.97 (d, 2H, ar, $J = 7.7$ Hz), 8.55 (s, 1H, H-3). Anal. Calc. for $C_{22}H_{23}N_7$.

7-Amino-5-(4-phenylethylpiperazin-1-yl)-2-phenyl-2H-pyrazolo[4,3-d]pyrimidine 17 The reaction mixture was microwave irradiated at 150 °C for 1 h. Column chromatography: eluent EtOAc/CH_2Cl_2/MeOH, 8:3:1. Yield 65%; m.p. 198–200 °C (cyclohexane/EtOAc). ^{1}H NMR (DMSO-d_6) 2.63–2.70 (m, 6H, 4 piperazine protons + CH_2), 2.87–2.91 (m, 2H, CH_2), 3.88–3.90 (m, 4H, piperazine protons), 5.53 (br s, 2H, NH_2), 7.23–7.34 (m, 5H, ar), 7.41 (t, 1H, ar, $J = 7.4$ Hz), 7.53 (t, 2H, ar, $J = 8.2$ Hz), 7.81 (d, 2H, ar, $J = 7.6$ Hz), 8.08 (s, 1H, H-3). Anal. Calc. for $C_{23}H_{25}N_7$.

7-Amino-5-(4-(2,4,6-trifluoro)benzylpiperazin-1-yl)-2-phenyl-2H-pyrazolo[4,3-d]pyrimidine 18 The reaction mixture was microwave irradiated at 150 °C for 1 h and 45 min. Column chromatography: eluent cyclohexane/EtOAc 7:3. Yield 85%; m.p. 233–235 °C (cyclohexane/EtOAc). ^{1}H NMR (DMSO-d_6) 2.43 (br s, 4H, piperazine protons), 3.57 (s, 2H, CH_2), 3.67 (br s, 4H, piperazine protons), 7.20 (t, 1H, ar, $J = 8.3$ Hz), 7.41 (t, 2H, ar, $J = 7.2$ Hz), 7.50 (br s, 2H, NH_2), 7.56 (t, 2H, ar, $J = 7.7$ Hz), 7.97 (d, 2H, ar, $J = 8.0$ Hz), 8.55 (s, 1H, H-3). Anal. Calc. for $C_{22}H_{20}N_7F_3$.

7-Amino-5-(4-(2-chloro-4-fluoro)benzylpiperazin-1-yl)-2-phenyl-2H-pyrazolo[4,3-d]pyrimidine 19 The reaction mixture was microwave irradiated at 150 °C for 1 h and 15 min. Column chromatography: eluent cyclohexane/EtOAc 7:3. Yield 53%; m.p. 203–205 °C. ^{1}H NMR (DMSO-d_6) 2.47 (br s, 4H, piperazine protons), 3.57 (s, 2H, CH_2), 3.70 (br s, 4H, piperazine protons), 7.24 (t, 1H, ar, $J = 6.2$ Hz), 7.41–7.60 (m, 7H, ar + NH_2), 7.98 (d, 2H, ar, $J = 7.8$ Hz), 8.56 (s, 1H, H-3). Anal. Calc. for $C_{22}H_{21}N_7ClF$.

7-Amino-2-phenyl-5-[(4-(2-furoyl)piperazin-1-yl]-2H-pyrazolo[4,3-d]pyrimidine 20 The reaction mixture was microwave irradiated at 150 °C for 1 h. Preparative TLC: eluent cyclohexane/EtOAc/MeOH 3:6:1. Yield 84%; m.p. 263–264 °C (EtOH). ^{1}H NMR (DMSO-d_6) 3.74–3.79 (m, 8H, CH_2), 6.65–6.66 (m, 1H, furan proton), 7.03–7.04 (m, 1H, furan proton), 7.42 (t, 1H, ar, $J = 7.4$ Hz), 7.51 (br s, 2H, NH_2), 7.57 (t, 2H, ar, $J = 7.8$ Hz), 7.87 (m, 1H, furan proton), 7.99 (d, 2H, ar, $J = 7.6$ Hz), 8.60 (s, 1H, H-3). Anal. Calc. for $C_{20}H_{19}N_7O_2$.

Tert-butyl 4-(7-amino-2-phenyl-2H-pyrazolo[4,3-d]pyrimidin-5-yl)piperazine 1-carboxylate 21 The reaction mixture was microwave irradiated at 150 °C for 1 h and 30 min. Column chromatography: eluent cyclohexane/EtOAc 6:4. Yield 76%; m.p. 169–171 °C. ^{1}H NMR (DMSO-d_6) 1.43 (s, 9H, t-But), 3.34–3.38 (m, 4H, piperazine protons), 3.63–3.68 (m, 4H, piperazine protons), 7.42 (t, 1H, ar, $J = 7.3$ Hz), 7.50 (br s, 2H, NH_2), 7.57 (t, 2H, ar, $J = 7.8$ Hz), 7.99 (d, 2H, ar, $J = 8.2$ Hz), 8.59 (s, 1H, H-3). Anal. Calc. for $C_{20}H_{25}N_7O_2$.

Synthesis of 2-phenyl-5-(4-(methyl-2-furyl)piperazin-1-yl)-2H-pyrazolo[4,3-d]pyrimidin-7-amine 22

A solution of the 5-(4-(2-furoyl)piperazin-1-yl) derivative **20** (1 mmol) in anhydrous THF (5 mL) was added to a suspension of $LiAlH_4$ (3 mmol) in anhydrous THF (20 mL) at 0 °C. The suspension was stirred for 16 h at room temperature, then treated with water (10 mL) and the solid which precipitated was filtered off. The clear solution was diluted with water (about 30 mL) and extracted with EtOAc (3 × 20 mL). The organic phase was anhydrified and the solvent removed at reduced pressure to give a solid which was purified by preparative TLC (eluent: cyclohexane/EtOAc/MeOH 5:5:0.4). Yield 65%; m.p. 199–200 °C. ^{1}H NMR (DMSO-d_6) 2.40–2.43 (m, 4H, piperazine protons), 3.53 (s, 2H, CH_2), 3.67–3.69 (m, 4H, piperazine protons), 6.30–6.32 (m, 1H, furan proton), 6.41–6.43 (m, 1H, furan proton), 7.38–7.43 (m, 3H, 1 ar + NH_2), 7.56–7.70 (m, 3H, 2 ar +1 furan proton), 7.98 (d, 2H, ar, $J = 7.4$ Hz), 8.54 (s, 1H, H-3). Anal. Calc. for $C_{20}H_{21}N_7O$.

Synthesis of 1-(2,4,6-trifluorobenzyl)piperazinium trifluoroacetate 60

A solution of N-(Boc)piperazine **63** (2.06 mmol) and 2,4,6-trifluorobenzaldehyde (1.87 mmol) in anhydrous CH_2Cl_2 (20 mL) was stirred at room temperature for 1.5 h, then triacetoxy sodium borohydride (7.47 mmol) was added portion wise. The mixture was refluxed for 48 h, then treated with iced water (10 mL) and diluted with CH_2Cl_2 (15 mL). The aqueous phase was extracted with CH_2Cl_2 (10 mL $\times 3$) and the organic phases were collected and anhydrified (Na_2SO_4). Evaporation of the solvent at reduced pressure gave the crude tert-butyl-4–(2,4,6-trifluorobenzyl)piperazine-1-carboxylate which was purified by preparative TLC (eluent: CH_2Cl_2/acetonitrile/cyclohexane, 9:1:1) and obtained as a yellow oil. Yield 91%; ^{1}H NMR ($CDCl_3$) 1.46 (s, 9H, t-But), 2.41–2.45 (m, 4H, piperazine protons), 3.42–3.46 (m, 4H, piperazine protons), 3.67 (s, 2H, CH_2), 6.69 (t, 2H, ar, $J = 7.8$ Hz).

This derivative was then transformed into the title compound as follows. A solution of concentrated trifluoroacetic acid (2.5 mL) in anhydrous CH_2Cl_2 (2.5 mL) was added dropwise to a solution of tert-butyl-4–(2,4,6-trifluorobenzyl)piperazine-1-carboxylate (1.04 mmol) in anhydrous CH_2Cl_2 (20 mL). The solution was stirred at room temperature for 3 h, then the solvent and the excess of the acid were removed at reduced pressure. The residue was treated with Et_2O (5 mL) to give a solid which was collected by filtration and dried. The crude compound was used for the next step without further purification. Yield 67%; ^{1}H NMR ($CDCl_3$) 2.29–3.31 (m, 4H, piperazine protons), 3.49–3.52 (m, 4H, piperazine protons), 4.12 (s, 2H, CH_2), 6.73 (t, ar, $J = 7.8$ Hz).

Synthesis of 4-(7-amino-2-phenyl-2H-pyrazolo[4,3-d]pyrimidin-5-yl)piperazin-1-ium trifluoroacetate 64

The title compound was obtained by treatment of compound **21** (1.04 mmol) with trifluoroacetic acid, in the conditions described previously to prepare compound **60** from the corresponding N-Boc-derivative. The crude compound was used directly for the next step without purification. Yield 68%; ^{1}H NMR (DMSO-d_6) 3.22–3.29 (m, 4H, piperazine protons), 3.98–4.02 (m, 4H, piperazine protons), 7.51 (t, 1H, ar, $J = 7.3$ Hz), 7.63 (t, 2H, ar, $J = 7.8$ Hz), 8.03 (d, 2H, ar, $J = 8.2$ Hz), 8.69 (s, 1H, H-3), 9.25 (br s, 2H, NH_2^+).

General procedure for the synthesis of 5–(4-acylpiperazin-1-yl)substituted-2H-pyrazolo[4,3-d]pyrimidin-7-amines 23 and 24

A mixture of derivative **64** (0.98 mmol) and triethylamine (1.96 mmol) in anhydrous THF (20 ml) was stirred at room temperature for 1 h. Then, 3,3-dimethylbutiryl chloride (1.17 mmol) or phenylacetyl chloride (1.17 mmol) was added and the solution was stirred at room temperature for 5 h or 3 h, respectively. The mixture was diluted with water (15 ml) and extracted with EtOAc (20 $\times$ 3 ml). The organic phase was anhydrified (Na_2SO_4) and the solvent evaporated at reduced pressure to give a solid which was taken up with cyclohexane and EtOAc, collected by filtration and purified by column chromatography (eluent $CHCl_3$/MeOH 10:0.5 for compound **23**, MeOH for derivative **24**).

7-Amino-2-phenyl-5-(4-(3,3-dimethylbutiryl)piperazin-1-yl)-2H-pyrazolo[4,3-d]pyrimidine 23 Yield 32%; m.p. 178–180 °C. ^{1}H NMR (DMSO-d_6) 1.02 (s, 9H, t-But), 2.29 (s, 2H, CH_2), 3.58–3.60 (m, 4H, piperazine protons), 3.69–3.72 (m, 4H, piperazine protons), 7.42–7.46 (m, 3H, 1 ar + NH_2) 7.59 (t, 2H, ar, $J = 7.4$ Hz), 8.00 (d, 2H, ar, $J = 7.9$ Hz), 8.60 (s, 1H, H-3). Anal. Calc. for $C_{21}H_{27}N_7O$.

7-Amino-2-phenyl-5-(4-phenylacetylpiperazin-1-yl)-2H-pyrazolo[4,3-d]pyrimidine 24 Yield 69%; m.p. 207–209 °C (CH_3NO_2). ^{1}H NMR (DMSO-d_6) 3.52–3.57 (m, 4H, piperazine protons), 3.60–3.66 (m, 4H, piperazine protons), 3.77 (s, 2H, CH_2), 7.21–7.34 (m, 5H, ar), 7.42–7.50 (m, 3H, 1 ar + NH_2), 7.57 (t, 2H, ar, $J = 7.9$ Hz), 7.98 (d, 2H, ar, $J = 8.2$ Hz), 8.59 (s, 1H, H-3). Anal. Calc. for $C_{23}H_{23}N_7O$.

Molecular modeling studies

Software overview

MOE suite (Molecular Operating Environment, version 2015.1001)[39] was used to perform most general molecular modeling operations.

Docking simulations were performed using the GOLD (Genetic Optimization for Ligand Docking, version 5.2) suite[40]. Quantum mechanical calculation of PM3 charges was carried out with the software MOPAC[41] as implemented in the MOE suite.

Analyses of docking poses in terms of energy calculation and visual inspection were executed taking advantage of the MOE suite.

Molecular modeling studies have been performed on a 8 CPU (Intel® Xeon® CPU E5-1620 3.70 GHz) linux workstation.

Three-dimensional structures of adenosine receptors

Among all the available crystallographic structures of hA_{2A} AR co-crystallized with a ligand in the orthosteric binding site, we opted for a complex with the antagonist ZM-241385 because of the structural similarity of its ([1,2,4]triazolo[1,5,*a*][1,3,5]triazin-5,7-yl)diamine scaffold with the (pyrazolo[4,3-*d*]pyrimidin-5,7-yl)diamine scaffold of the compounds under investigation. The crystallographic structure identified with 4EIY PDB code[42] was selected among all the structures co-crystallized with ZM-241385, because of its highest resolution (1.80 Å).

Since to date there are no crystallographic structures available for hA_3 and hA_1 ARs, we retrieved from the *Adenosiland* web-platform[43,44] previously developed by our research group, their homology models constructed using 4EIY structure as template. Those models were constructed in the presence of ZM-241385 as environment for induced fit, so the resulting structures consist in complexes between each AR subtype and the antagonist ZM-241385.

The residues are identified according to the generic Ballesteros Weinstein numbering system[45].

Molecular docking

Three-dimensional structures of ligands were built taking advantage of the MOE-Builder tool and ionization states were predicted using the MOE-Protonate-3D tool[46]. Ligand structures were subjected to MMFF94$\times$ energy minimization until the root mean square (rms) gradient fell below 0.05 kcal mol^{-1} Å^{-1}. GOLD docking tool[40] was selected as conformational search program and GoldScore as scoring function, thanks to a docking benchmark study previously carried out in our laboratory[38,47]. For each compound, 10 docking runs were performed on each receptor subtype, searching in a sphere of 20 Å radius centered on the coordinates of the center of mass of ZM-241385 in complex with the receptor. Along with the compounds under investigation, docking simulations were conducted also for ZM-241385 as a reference example.

After computing atomic partial charges both of ligand poses, using PM3/ESP method, and receptors, using Amber10EHT force field, electrostatic and van der Waals contributions to the binding energy were calculated with MOE.

Interaction energy fingerprints (IEFs)

Individual electrostatic and hydrophobic interactions, hereinafter identified as IEele and IEhyd, respectively, were computed between ligand poses and each protein residue involved in binding[37,38]. Both these contributions were computed using MOE and, in particular, IEele were calculated as non-bonded electrostatic interactions energy term of the force field, so they are expressed in kcal/mol. Instead, IEhyd were computed as contact hydrophobic surfaces and are associated to an adimensional score (the higher the better). The data obtained by this analysis were reported in a graphic, called Interaction Energy Fingerprints (IEFs), representing residues (*x*-axis) in the form of equally high rectangles rendered according to a colorimetric scale. As regards IEele, colors from blue to red represent energy values ranging from negative to positive values; for IEhyd, colors from white to dark green depict scores going from 0 to positive values. More precisely, we retrieved the coordinates of the center of mass of ZM-241385 in the structure of each AR subtype complex. Only residues within 10 Å from this point were retained as belonging to the binding site, and plotted in the IEFs.

Interaction Energy Fingerprints comparison (IEFs comparison)

A new method has been introduced to evaluate docking results, which rests on the observation that ligands able to bind the same site of a protein often share a similar interaction pattern, too. The new method consists in the comparison of the IEFs of the pose of a candidate ligand (hereinafter called "docked") with the IEFs of a ligand whose bound conformation is considered known (hereinafter called "reference").

A quantitative estimation of the similarity of IEFs is computed as root mean square deviation (RMSD) between per residue interaction energies of the docked and the reference poses, both for electrostatic and hydrophobic interactions. This would inform about the average divergence of the docked from the reference: in particular a high RMSD value corresponds to large differences.

So far, there is no information about the direction of the divergence thus, along with RMSD, another analysis, named $RMSD_{trend}$, has been proposed. This consists of the sum of differences between per residue interaction energies of the docked and the reference, weighted by the number of residues of the binding site. A more favorable interaction energy profile would correspond to a negative $RMSD_{trend}$ in the case of electrostatic interactions, while to a positive one in the case of hydrophobic interactions.

In summary, low RMSD values, along with negative electrostatic $RMSD_{trend}$ and high hydrophobic $RMSD_{trend}$ could be interpreted as an indication of a higher "stability" of the docked pose respect the reference in the orthosteric binding state.

Moreover, this approach could be expanded to compare the behavior of the same ligand on different receptor subtypes, in order to have a preliminary "selectivity" profile based on the stabilities of the docked poses in their corresponding orthosteric binding states. In that case, RMSD and $RMSD_{trend}$ are computed for a docked compound against a reference on each receptor subtype. The reference compound should be a known good binder for each subtype and, at best, the crystallographic structure of the complex should be known.

In our case, ZM-241385 was chosen as reference compound, since it is a ligand for all ARs, having a K_i of 774 nM for hA_1 AR, of 1.6 nM for hA_{2A} AR and of 743 nM for hA_3 AR[5]. As regards the hA_{2A} receptor, 4EIY crystallographic complex could be employed, while, for hA_1 and hA_3 ARs, we used the homology models, that are receptor-ZM-241385 complexes, since they were constructed considering ZM-241385 as environment for induced fit.

An additional graph was added, which allows to compare electrostatic and hydrophobic IEFs RMSDs and $RMSD_{trend}$ for different ligands on the different AR subtypes. RMSD and $RMSD_{trend}$ for the ligands (*y*-axis) on the various receptors (*x*-axis) were reported on a heat map, where they are represented by a colorimetric scale going from red to blue from unfavorable to favorable values. Finally, if a ligand presents blue rectangles on all receptors, it is expected to be "non-selective", otherwise red and blue rectangles should describe lower and higher stability values, respectively, among the different receptor subtypes.

MMsDocking video maker

To facilitate the visualization and analysis of data obtained from the docking simulations, we have implemented a in-house tool, named MMsDocking video maker, for the automated production of a video that shows the most relevant docking data, such as docking poses, per residue IEhyd and IEele data, experimental binding data and scoring values. Videos were mounted using MEncoder[48] starting from images obtained with the following procedure: the heat maps in the background were drawn with GNUPLOT 4.6[49] starting from per residue IEhyd and IEele data computed with MOE. 2d depictions of compounds were generated using the open-source cheminformatics toolkit RD*Kit*[50]. Representations of docking poses within the binding site were constructed using CHIMERA[51].

Pharmacological assays

Human cloned A_1, A_{2A} and A_3 AR binding assay

All synthesized compounds were tested to evaluate their affinity at human A_1, A_{2A} and A_3 ARs. Displacement experiments of [^{3}H]DPCPX (1 nM) to hA_1 CHO membranes (50 μg of protein/assay) and at least 6–8 different concentrations of antagonists for 120 min at 25 °C in 50 mM Tris-HCl buffer pH 7.4 were performed[52]. Non-specific binding was determined in the presence 1 μM of DPCPX (≤10% of the total binding). Binding of [^{3}H]ZM-241385 (1 nM) to hA_{2A}CHO membranes (50 μg of protein/assay) was performed by using 50 mM Tris-HCl buffer, 10 mM $MgCl_2$ pH 7.4 and at least 6–8 different concentrations of antagonists studied for an incubation time of 60 min at 4 °C[53]. Non-specific binding was determined in the presence of 1 μM ZM-241385 and was about 20% of total binding. Competition binding experiments to hA_3 CHO membranes (50 μg of protein/assay) were performed incubating 0.5 nM [^{125}I]AB-MECA, 50 mM Tris-HCl buffer, 10 mM $MgCl_2$, 1 mM EDTA, pH 7.4 and at least 6–8 different concentrations of examined ligands for 60 min at 37 °C[54]. Non-specific binding was defined as binding in the presence of 1 μM AB-MECA and was about 20% of total binding. Bound and free radioactivity were separated by filtering the assay mixture through Whatman GF/B glass fiber filters by using a Brandel cell harvester. The filter bound radioactivity was counted by Scintillation Counter Packard Tri Carb 2810 TR with an efficiency of 58%.

Measurement of cyclic AMP levels in CHO cells transfected with hA_{2B} AR

CHO cells transfected with hA_{2B} AR subtypes were washed with phosphate-buffered saline, diluted trypsin and centrifuged for 10 min at 200 *g*. The cells (1×10^6 cells/assay) were suspended in 0.5 ml of incubation mixture (mM): NaCl 15, KCl 0.27, NaH_2PO_4

0.037, $MgSO_4$ 0.1, $CaCl_2$ 0.1, Hepes 0.01, $MgCl_2$ 1, glucose 0.5, pH 7.4 at 37 °C, 2 IU/ml adenosine deaminase and 4–(3-butoxy-4-methoxybenzyl)-2-imidazolidinone (Ro 20–1724) as phosphodiesterase inhibitor and preincubated for 10 min in a shaking bath at 37 °C. The potency of antagonists to the A_{2B} AR was determined by the inhibition of NECA (200 nM)-induced cyclic AMP production[55]. The reaction was terminated by the addition of cold 6% trichloroacetic acid (TCA). The TCA suspension was centrifuged at 2000 *g* for 10 min at 4 °C and the supernatant was extracted four times with water saturated diethyl ether. The final aqueous solution was tested for cyclic AMP levels by a competition protein binding assay. Samples of cyclic AMP standard (0–10 pmoles) were added to each test tube containing [^{3}H] cyclic AMP and incubation buffer (trizma base 0.1 M, aminophylline 8.0 mM, 2-mercaptoethanol 6.0 mM, pH 7.4). The binding protein prepared from beef adrenals was added to the samples previously incubated at 4 °C for 150 min, and, after the addition of charcoal, was centrifuged at 2000 *g* for 10 min. The clear supernatant was counted in a Scintillation Counter Packard Tri Carb 2810 TR with an efficiency of 58%.

Data analysis

The protein concentration was determined according to a Bio-Rad method[56] with bovine albumin as a standard reference. Inhibitory binding constant (K_i) values were calculated from those of IC_{50} according to Cheng & Prusoff equation $K_i = IC_{50}/(1 + [C^*]/K_D^*)$, where [C*] is the concentration of the radioligand and K_D^* its dissociation constant[57]. A weighted non-linear least-squares curve fitting program LIGAND[58] was used for computer analysis of inhibition experiments. IC_{50} values obtained in cyclic AMP assay were calculated by non-linear regression analysis using the equation for a sigmoid concentration–response curve (Graph-PAD Prism, San Diego, CA).

Disclosure statement

The authors report no declarations of interest.

Funding

The synthetic work was financially supported by the University of Florence, Italy, the Italian Ministry for University and Research (MIUR, PRIN 2010–2011, 20103W4779_004 project). The molecular modeling work coordinated by S.M. was carried out with financial support from the University of Padova, Italy, and the Italian Ministry for University and Research (MIUR), Rome, Italy. S.M. is also very grateful to Chemical Computing Group and to OpenEye for the scientific and technical partnership.

References

1. Fredholm BB, IJzerman AP, Jacobson KA, et al. International union of pharmacology XXV. Nomenclature and classification of adenosine receptors. Pharmacol Rev 2001;53:527–52.
2. Fredholm BB, IJzerman AP, Jacobson KA, et al. International union of pharmacology LXXXI. Nomenclature and classification of adenosine receptors. An up date. Pharmacol Rev 2011;63:1–34.
3. Maemoto T, Tada M, Mihara T, et al. Pharmacological characterization of FR194921, a new potent, selective, and orally active antagonist for central adenosine A_1 receptors. J Pharmacol Sci 2004;96:42–52.
4. Mihara T, Iwashita A, Matsuoka N. A novel adenosine A_1 and A_{2A} receptor antagonist ASP5854 ameliorates motor impairment in MPTP-treated marmosets: comparison with existing anti-Parkinson's disease drugs. Behav Brain Res 2008;194:152–61.
5. Jacobson KA, Gao Z-G. Adenosine receptors as therapeutic targets. Nat Rev Drug Discov 2006;5:247–64.
6. Navarro G, Borroto-Escuela DO, Fuxe K, Franco R. Purinergic signaling in Parkinson's disease. Relevance for treatment. Neuropharmacology 2016;104:161–8.
7. Armentero MT, Pinna A, Ferré S, et al. Past, present and future of A_{2A} adenosine receptor antagonists in the therapy of Parkinson's disease. Pharmacol Ther 2011;132:280–99.
8. Chen J-F, Eltzschig HK, Fredholm BB. Adenosine receptors as drug targets — what are the challenges? Nat Rev Drug Discov 2013;12:265–86.
9. Kyowa Hakko K. Approval for manufacturing and marketing of NOURIAST tablets 20 mg. A novel antiparkinsonian agent; 2013. Available from: http://www.kyowakirin.com/news releases/2013/e20130325_04.htlm.
10. Shook BC, Rassnick S, Wallace N, et al. Design and characterization of optimized adenosine A_{2A}/A_1 receptor antagonists for the treatment of Parkinson's disease. J Med Chem 2012;55:1402–17.
11. Shook BC, Rassnick S, Jackson PF, et al. JNJ-40255293, a novel adenosine A_{2A}/A_1 antagonist with efficacy in preclinical models of Parkinson's disease. ACS Chem Neurosci 2014;5:1005–19.
12. Preti D, Baraldi PG, Moorman AR, et al. History and perspectives of A_{2A} adenosine receptor antagonists as potential therapeutic agents. Med Res Rev 2015;35:790–848.
13. Perez-Aso M, Chiriboga L, Cronstein BN. Pharmacological blockade of adenosine A_{2A} receptors diminishes scarring. FASEB J 2012;26:4254–63.
14. Leone RD, Lo Y-C, Powell JD. A_{2A}R antagonists: next generation checkpoint blockade for cancer immunotherapy. Comput Struct Biotechnol J 2015;13:265–72.
15. Catarzi D, Colotta V, Varano F, et al. 1,2,4-Triazolo[1,5-a]quinoxaline as a versatile tool for the design of selective human A_3 adenosine receptor antagonists: synthesis, biological evaluation and molecular modeling studies of 2-(hetero)aryl- and 2-carboxy-substituted derivatives. J Med Chem 2005;48:7932–45.
16. Lenzi O, Colotta V, Catarzi D, et al. 4-Amido-2-aryl-1,2,4-triazolo[4,3-a]quinoxalin-1-ones as new potent and selective human A_3 adenosine receptor antagonists. Synthesis, pharmacological evaluation and ligand-receptor modeling studies. J Med Chem 2006;49:3916–25.
17. Morizzo E, Capelli F, Lenzi O, et al. Scouting human A_3 adenosine receptor antagonist binding mode using a molecular simplification approach: from triazoloquinoxaline to a pyrimidine skeleton as a key study. J Med Chem 2007;50:6596–606.
18. Colotta V, Catarzi D, Varano F, et al. Synthesis, ligand-receptor modeling studies and pharmacological evaluation of novel 4-modified-2-aryl-1,2,4-triazolo[4,3-a]quinoxalin-1-one derivatives as potent and selective human A_3 adenosine receptor antagonists. Bioorg Med Chem 2008;16:6086–102.
19. Colotta V, Lenzi O, Catarzi D, et al. Pyrido[2,3-*e*]-1,2,4-triazolo[4,3-a]pyrazin-1-one as a new scaffold to develop potent and selective human A_3 adenosine receptor antagonists. Synthesis, pharmacological evaluation and ligand-receptor modeling studies. J Med Chem 2009;52:2407–19.

20. Lenzi O, Colotta V, Catarzi D, et al. 2-Phenylpyrazolo[4,3-*d*]pyrimidin-7-one as a new scaffold to obtain potent and selective human A_3 adenosine receptor antagonists: new insights into the receptor-antagonist recognition. J Med Chem 2009;52:7640–52.
21. Poli D, Catarzi D, Colotta V, et al. The identification of the 2-phenylphthalazin-1(2H)-one scaffold as a new decorable core skeleton for the design of potent and selective human A_3 adenosine receptor antagonists. J Med Chem 2011;54:2102–13.
22. Squarcialupi L, Colotta V, Catarzi D, et al. 2-Arylpyrazolo[4,3-*d*]pyrimidin-7-amino derivatives as new potent and selective human A_3 adenosine receptor antagonists. Molecular modeling studies and pharmacological evaluation. J Med Chem 2013;56:2256–69.
23. Catarzi D, Colotta V, Varano F, et al. Pyrazolo[1,5-c]quinazoline derivatives and their simplified analogues as adenosine receptor antagonists: synthesis, structure–affinity relationships and molecular modeling studies. Bioorg Med Chem 2013;21:283–94.
24. Squarcialupi L, Colotta V, Catarzi D, et al. 7-Amino-2-phenylpyrazolo[4,3-*d*]pyrimidine derivatives: structural investigations at the 5-position to target A_1 and A_{2A} adenosine receptors. Molecular modeling and pharmacological studies. Eur J Med Chem 2014;84:614–27.
25. Varano F, Catarzi D, Squarcialupi L, et al. Exploring the 7-oxo-thiazolo[5,4-d]pyrimidine core for the design of new human adenosine A_3 receptor antagonists. Synthesis, molecular modeling studies and pharmacological evaluation. Eur J Med Chem 2015;96:105–21.
26. Squarcialupi L, Catarzi D, Varano F, et al. Structural refinement of pyrazolo[4,3-*d*]pyrimidine derivatives to obtain highly potent and selective antagonists for the human A_3 adenosine receptor. Eur J Med Chem 2016;108:614–27.
27. Federico S, Paoletta S, Cheong SL, et al. Synthesis and biological evaluation of a new series of 1,2,4-triazolo[1,5-*a*]-1,3,5-triazines as human A_{2A} adenosine receptor antagonists with improved water solubility. J Med Chem 2011;54:877–89.
28. Vu CB, Pan D, Peng B, et al. Novel diamino derivatives of [1,2,4]triazolo[1,5-a][1,3,5]triazine as potent and selective adenosine A_{2A} receptor antagonists. J Med Chem 2005;48:2009–18.
29. Wong R, Dolman SJ. Isothiocyanates from tosyl chloride mediated decomposition of in situ generated dithiocarbamic acid salts. J Org Chem 2007;72:3969–71.
30. Gittos MW, Robinson MR, Verge JP, et al. Intramolecular cyclization of arylalkyl isothiocyanates. I. Synthesis of 1-substituted 3,4-dihydroisoquinolines. J Chem Soc Perkin Trans 1 Org Bioorg Chem 1976;1:33–8.
31. Antos K, Nemec P, Hrdina M. 4-Substituted β-Phenylethylisothiocyanates. Collect Czech Chem Comm 1972;37:3339–41.
32. Brown GB, Weliky VS. 2-Chloroadenine and 2-chloroadenosine. J Org Chem 1958;23:125–6.
33. Oumata N, Bettayeb K, Ferandin Y, et al. Roscovitine-derived, dual-specificity inhibitors of cyclin-dependent kinases and casein kinases 1. J Med Chem 2008;51:5229–42.
34. Lee W, Ortwine DF, Bergeron P, et al. A hit to lead discovery of novel N-methylated imidazolo-, pyrrolo-, and pyrazolo-pyrimidines as potent and selective mTOR inhibitors. Bioorg Med Chem Lett 2013;23:5097–104.
35. Kanojia RM, Salata JJ, Kauffman J. Synthesis and class III type antiarrhythmic activity of 4-aroyl (and aryl)-1-aralkylpiperazines. Bioorg Med Chem Lett 2000;10:2819–923.
36. Meyer WE, Tomcufcik AS, Chan PS, Haug M. 5-(1-Piperazinyl)-1H-1,2,4-triazol-3-amines as antihypertensive agents. J Med Chem 1989;32:593–7.
37. Ciancetta A, Sabbadin D, Federico S, et al. Advances in computational techniques to study GPCR-ligand recognition. Trends Pharmacol Sci 2015;36:878–90.
38. Ciancetta A, Cuzzolin A, Moro S. Alternative quality assessment strategy to compare performances of GPCR-ligand docking protocols: the human adenosine A_{2A} receptor as a case study. J Chem Inf Model 2014;54:2243–54.
39. Chemical Computing Group Inc. Molecular Operating Environment (MOE); 2016. [Internet]. Available from: http://www.chemcomp.com
40. Cambridge Crystallographic Data Centre: 12 Union Road, Cambridge CB2 1EZ, UK. GOLD suite, version 5.2; 2016. [Internet]; Available from: http://www.ccdc.cam.ac.uk.
41. Stewart JJ. Optimization of parameters for semiempirical methods V: modification of NDDO approximations and application to 70 elements. J Mol Model 2007;13:1173–213.
42. Liu W, Chun E, Thompson AA, et al. Structural basis for allosteric regulation of GPCRs by sodium ions. Science 2012;337:232–6.
43. Floris M, Sabbadin D, Medda R, et al. Adenosiland: walking through adenosine receptors landscape. Eur J Med Chem 2012;58:248–57.
44. Floris M, Sabbadin D, Ciancetta A, et al. Implementing the "Best Template Searching" tool into Adenosiland platform. In Silico Pharmacol 2013;20:1–25.
45. Ballesteros JA, Weinstein H. Integrated methods for the construction of three-dimensional models and computational probing of structure-function relations in G protein-coupled receptors. Methods Neurosci 1995; 25:366–428.
46. Labute P. Protonate3D: assignment of ionization states and hydrogen coordinates to macromolecular structures. Proteins 2009;75:187–205.
47. Cuzzolin A, Sturlese M, Malvacio I, et al. DockBench: an integrated informatic platform bridging the gap between the robust validation of docking protocols and virtual screening simulations. Molecules 2015;20:9977–93.
48. MEncoder; 2016. [Internet]. Available from: http://www.mplayerhq.hu/design7/projects.html.
49. Gnuplot; 2016. [Internet]. Available from: http://www.gnuplot.info/index.html.
50. RDKit: Cheminformatics and Machine Learning Software; 2016. [Internet]. Available from: http://www.rdkit.org.
51. Pettersen EF, Goddard TD, Huang CC, et al. UCSF chimera: a visualization system for exploratory research and analysis. J Comput Chem 2004;25:1605–12.
52. Borea PA, Dalpiaz A, Varani K, et al. Binding thermodynamics at A_1 and A_{2A} adenosine receptors. Life Sci 1996;59:1373–88.
53. Varani K, Rigamonti D, Sipione S, et al. Aberrant amplification of A_{2A} receptor signalling in striatal cells expressing mutant huntigtin. FASEB J 2001;5:1245–7.
54. Varani K, Cacciari B, Baraldi PG, et al. Binding affinity of adenosine receptor agonists and antagonists at human cloned A_3 adenosine receptors. Life Sci 1998;63:81–7.
55. Varani K, Gessi S, Merighi S, et al. Pharmacological characterization of novel adenosine ligands in recombinant and native human A_{2B} receptors. Biochem Pharmacol 2005;70:1601–12.

56. Bradford MM. A rapid and sensitive method for the quantification of microgram quantities of protein utilizing the principle of protein dye-binding. Anal Biochem 1976;72:248–54.
57. Prusoff CYC, Relationships WH. between the inhibition constant (K_i) and the concentration of inhibitor which causes 50 per cent inhibition (IC_{50}) of an enzymatic reaction. Biochem Pharmacol 1973;22:3099–108.
58. Munson PJ, Rodbard D. Ligand: a versatile computerized approach for the characterization of ligand binding systems. Anal Biochem 1980;107:220–39.